NACA

RESEARCH MEMORANDUM

EFFECT OF FREQUENCY OF SIDESLIPPING MOTION ON THE LATERAL STABILITY DERIVATIVES OF A TYPICAL DELTA-WING AIRPLANE

By Jacob H. Lichtenstein and James L. Williams

Langley Aeronautical Laboratory
Langley Field, Va.

NATIONAL ADVISORY COMMITTEE
FOR AERONAUTICS

WASHINGTON

September 12, 1957
Declassified April 15, 1958

NACA RM L57F07

NATIONAL ADVISORY COMMITTEE FOR AERONAUTICS

RESEARCH MEMORANDUM

EFFECT OF FREQUENCY OF SIDESLIPPING MOTION ON THE LATERAL STABILITY DERIVATIVES OF A TYPICAL DELTA-WING AIRPLANE

By Jacob H. Lichtenstein and James L. Williams

SUMMARY

An investigation has been made in the Langley stability tunnel at low speeds to determine the effect of frequency of sideslipping motion on the lateral stability derivatives of a 60° delta-wing airplane configuration.

The results of the investigation have shown that, for either the wing alone, the wing-fuselage combination, or the wing—fuselage—vertical-tail combination, changes in the frequency of oscillation generally had only minor effects on the stability derivatives at low angles of attack, with the exception of the yawing-moment derivatives of the wing—fuselage—vertical-tail configuration which exhibited a considerable effect of frequency. At the high angles of attack the magnitude of all the stability derivatives measured underwent very large changes as a result of the oscillatory motion.

It was also found that for the wing-alone configuration the leading-edge radius had a very pronounced bearing on the effects due to the oscillatory motion. Decreasing the leading-edge radius, for instance, considerably increased the magnitude of the effects due to changes in frequency.

The use of the oscillatory stability derivatives in calculating the period and time to damp to one-half amplitude, instead of the use of the steady-state derivatives, resulted in an increase in the indicated damping and stability for high angles of attack. It did, however, increase the time to damp somewhat at low angles.

INTRODUCTION

Recent developments have shown that stability derivatives obtained from oscillation tests can be considerably different from those obtained by steady-flow tests for some angle-of-attack and Mach number ranges (refs. 1, 2, and 3) and that these differences can be quite important in the calculation of the stability and motions of an airplane (ref. 4). It was also found that the magnitude of these measured oscillatory derivatives depended to a large extent upon the frequency and amplitude of the oscillatory motion (ref. 5).

A common and widely used oscillation technique is one wherein the model is simply oscillated about a fixed vertical (Z) axis relative to the model. These tests are commonly called oscillation-in-yaw tests, and yield a derivative that is a combination of two terms; for example, the damping term consists of the damping in yaw C_{n_r} and an acceleration-in-sideslip term $C_{n_{\dot{\beta}}}$ in the combination $C_{n_r} - C_{n_{\dot{\beta}}}$. However, in the equations used for calculating the airplane motion, these two derivatives are needed separately. Techniques have recently been developed at the Langley stability tunnel which will permit the measurement of the yaw and sideslip terms independently. Oscillatory tests in pure yawing, as described in reference 6, involve a snaking motion in which there is no sideslip, and oscillatory tests in pure sideslip involve a side-to-side motion in which there is no rotation (ref. 3).

Presented in this paper is a low-speed investigation of pure sideslipping motion on a 60° delta wing alone and in combination with a fuselage and vertical tail. The range of reduced frequencies of oscillation varied from 0.066 to 0.218 at a maximum amplitude of sideslip of ±2°, and the angle of attack varied from 0° to 32°. For comparison with the wing which had an NACA 65A003 airfoil section, a flat-plate 60° delta wing also was tested in sideslipping motion. In addition to the sideslipping tests some results are reported for oscillation-in-yaw tests (e.g., $C_{n_r} - C_{n_{\dot{\beta}}}$ derivative) for both of the wings. Computations of the period and time to damp to one-half amplitude were made using the measured oscillation sideslip data. These computations were made for a typical delta-wing airplane.

SYMBOLS

The data are presented in the form of standard NACA coefficients of forces and moments which are referred to the stability system of axes with the origin at the projection on the plane of symmetry of the quarter-chord point of the mean aerodynamic chord. The positive direction of

forces, moments, angular displacements, and velocities are shown in figure 1. The coefficients and symbols used are defined as follows:

C_L lift coefficient, $\frac{\text{Lift}}{qS_w}$

C_D drag coefficient, $\frac{\text{Drag}}{qS_w}$

C_Y lateral-force coefficient, $\frac{\text{Lateral force}}{qS_w}$

C_l rolling-moment coefficient, M_X/qS_wb_w

C_n yawing-moment coefficient, M_Z/qS_wb_w

C_m pitching-moment coefficient, $M_Y/qS_w\bar{c}_w$

M_X rolling moment, ft-lb

M_Z yawing moment, ft-lb

M_Y pitching moment, ft-lb

q dynamic pressure, $\frac{1}{2}\rho V^2$, lb/sq ft

ρ mass density of air, slugs/cu ft

V free-stream velocity, ft/sec

S area, sq ft

b span, ft

c chord, ft

$\bar{c}$ mean aerodynamic chord, $\frac{2}{S}\int_0^{b/2} c^2\,dy$, ft

l_v distance from origin of axis to $\bar{c}/4$ of tail, ft

d maximum fuselage diameter

X,Y,Z stability axis system

y displacement along Y-axis, ft

y_o maximum sidewise displacement, ft

$\dot{y},v$ velocity along the Y-axis, $\frac{\partial y}{\partial t}$, ft/sec

$\ddot{y},\dot{v}$ acceleration along the Y-axis, $\frac{\partial \dot{y}}{\partial t}$, ft/sec^2

α angle of attack with respect to wing chord plane, deg

β angle of sideslip, $\tan^{-1}\frac{v}{V}$, radians unless otherwise specified

$\dot{\beta} = \frac{\partial \beta}{\partial t} = \frac{\dot{v}}{V}$ radians/sec

ω angular velocity, $2\pi f$, radians/sec

ψ angle of yaw, radians

γ mass unbalance about mounting point, slug-ft^2

f frequency, cps

t time, sec

$\frac{\omega b}{2V}$ reduced frequency parameter

$\frac{\dot{\beta} b}{2V}$ sideslipping-acceleration parameter referred to semispan of wing

$\frac{rb}{2V}$ yawing-velocity parameter referred to semispan of wing

$\frac{pb}{2V}$ rolling-velocity parameter referred to semispan of wing

r yawing velocity, $\frac{\partial \psi}{\partial t}$, radians/sec

$\dot{r}$ yawing acceleration, $\frac{\partial^2 \psi}{\partial t^2}$, radians/sec^2

p rolling angular velocity, radians/sec

$C_{l_\beta} = \frac{\partial C_l}{\partial \beta}$

$$C_{n_\beta} = \frac{\partial C_n}{\partial \beta}$$

$$C_{Y_\beta} = \frac{\partial C_Y}{\partial \beta}$$

$$C_{l_{\dot{\beta}}} = \frac{\partial C_l}{\partial\left(\frac{\dot{\beta} b}{2V}\right)}$$

$$C_{n_{\dot{\beta}}} = \frac{\partial C_n}{\partial\left(\frac{\dot{\beta} b}{2V}\right)}$$

$$C_{l_r} = \frac{\partial C_l}{\partial\left(\frac{rb}{2V}\right)}$$

$$C_{n_r} = \frac{\partial C_n}{\partial\left(\frac{rb}{2V}\right)}$$

$$C_{l_{\dot{r}}} = \frac{\partial C_l}{\partial\left(\frac{\dot{r} b^2}{4V^2}\right)}$$

$$C_{n_{\dot{r}}} = \frac{\partial C_n}{\partial\left(\frac{\dot{r} b^2}{4V^2}\right)}$$

$$C_{l_p} = \frac{\partial C_l}{\partial\left(\frac{pb}{2V}\right)}$$

$$C_{n_p} = \frac{\partial C_n}{\partial\left(\frac{pb}{2V}\right)}$$

$$C_{Y_r} = \frac{\partial C_Y}{\partial\left(\frac{rb}{2V}\right)}$$

$$C_{Y_p} = \frac{\partial C_Y}{\partial\left(\frac{pb}{2V}\right)}$$

P period of oscillation, sec

$T_{1/2}$ time to damp to one-half amplitude, $\frac{-0.693}{\lambda'}\frac{\mu b}{V}$, sec

T_2 time to double amplitude, $\frac{0.693}{\lambda'}\frac{\mu b}{V}$, sec

λ' nondimensional root of lateral-stability-characteristic equation (ref. 7)

μ airplane relative density, $\frac{W}{g\rho Sb}$

W airplane weight, lb

g acceleration due to gravity, ft/sec^2

$$M_{Z_{\ddot{y}}} = \frac{\partial M_Z}{\partial \ddot{y}}$$

$$M_{Z_{\dot{y}}} = \frac{\partial M_Z}{\partial \dot{y}}$$

$$M_{X_{\ddot{y}}} = \frac{\partial M_X}{\partial \ddot{y}}$$

$$M_{X_{\dot{y}}} = \frac{\partial M_X}{\partial \dot{y}}$$

Subscripts:

v vertical tail

w wing

ω oscillatory

MODELS AND APPARATUS

Models

The model used in the majority of the tests of this investigation is shown in figure 2 and pertinent geometric information is given in tables I and II. The configuration is, in general, fairly typical of a delta-wing airplane; the wing had an aspect ratio of 2.31, a 60° swept-back leading edge, and an NACA 65A003 airfoil section. The fuselage was a body of revolution pointed at the nose and blunt at the rear to simulate a jet configuration. The vertical tail was triangular, of aspect ratio 2.18, and had a leading-edge sweepback of 42.5° and an NACA 65-006 airfoil section. A photograph of the complete model mounted in the 6- by 6-foot test section of the Langley stability tunnel is shown in figure 3.

The model had separable wing, fuselage, and tail surfaces in order to facilitate testing of the model as a whole and as components. The components were made of balsa wood covered with a thin layer of fiber glass in order to minimize the mass and make the natural frequency of the model on its mounting as high as possible. An attempt was made to balance the model in pitch, roll, and yaw in order to decrease the out-of-balance moments.

Some tests were made with another wing which had the same plan form as the basic wing but had a flat-plate airfoil section with a thickness ratio of 2.4 percent based on the chord and rounded leading edge with a radius of one-half the thickness. The trailing edge was beveled to give a 10° trailing-edge angle.

Apparatus

The apparatus used in this investigation for oscillation in sideslip is similar to that used in reference 3, except that the oscillatory motion of the apparatus was forced at a constant amplitude for these tests and the oscillatory motion was free to damp in the tests of reference 3. The oscillating portion of this apparatus (oscillating support strut) shown in figures 4(a) and (b) consisted of a 9-foot length of streamlined steel tubing which spanned the tunnel jet and extended through the walls of the 6- by 6-foot test section of the Langley stability tunnel. The ends of this streamlined strut were supported by triangular-shaped swinging arms, which were pivoted and supported by rigid tunnel structural members. The oscillating motion was imparted to the strut by the push rod which had one end pinned to the strut and the other end mounted off center on the rotating flywheel (fig. 4(b)). The location of the push-rod attachment at the flywheel could be changed so that the amplitude of the motion could be adjusted

to give the desired sideslipping velocity for a given frequency. The off-center mass of the attachment was balanced by a lead weight mounted on the flywheel. The inertia of the flywheel was made large in order to reduce, as much as practical, the fluctuations in circular velocity that occur during a cycle. The flywheel was driven by a 1-horsepower direct-current motor through a gear drive system with a reduction ratio of 6 to 1 (fig. 4(c)). The frequency of the oscillation was controlled by varying the voltage to the drive motor.

A pure lateral oscillatory motion cannot be obtained with such an apparatus; however, by using a swinging-arm radius of 45 inches, the streamwise motion of the model can be considered negligible (about 3/4 of 1 percent of free-stream velocity). A sketch depicting typical motion of the model is given in figure 5. Because of the eccentricity of the crank arm, the resulting motion is not a true sinusoidal motion. The distortion varies from zero at the ends of the motion to a maximum at the center of the motion. The data-reduction system (ref. 6) was such that the error at the maximum distortion was less than 1 percent for the worst case and the average error over an entire cycle was considered to be negligible.

The model was raised above the horizontal strut in order to reduce the interference of the strut on the model (fig. 3). The rolling and yawing moments were measured by a two-component strain gage located at the desired center of gravity of the model. The output from the strain gage was fed to a data-reduction system which permitted readings of the in-phase and out-of-phase portions of the total moment on a meter. This data-reduction system is described in detail in the appendix of reference 6 and therefore will not be described herein.

The apparatus used for the oscillation-in-yaw tests was the same as that described in reference 5. The data-reduction equipment was the same as that used for the oscillation-in-sideslip tests. For the steady-state tests the conventional six-component mechanical balance system was used with the models mounted on a single strut support.

TESTS AND CORRECTIONS

Tests

The tests were conducted in the 6- by 6-foot test section of the Langley stability tunnel at a dynamic pressure of 24.9 pounds per square foot. This corresponds to a Mach number of 0.13 and a Reynolds number of about 1.6×10^6 based upon the mean aerodynamic chord of the wing.

The oscillation-in-sideslip tests were made for three basic model configurations, the NACA 65A003 airfoil wing, the wing-fuselage combination, the wing—fuselage—vertical-tail combination. The angle-of-attack range was varied from 0° to 32° (0° to 16° in 4° increments and 16° to 32° in 2° increments). The basic model configurations were tested at one amplitude of sideslipping oscillation, ±2° for four frequencies (1, 1.65, 2.00, and 3.31 cycles per second) which corresponds to reduced frequency parameters $\frac{\omega b}{2V}$ of 0.066, 0.109, 0.132, and 0.218, respectively.

Some additional tests were made on a flat-plate wing. This wing was tested at the same amplitude of oscillation (±2°) and angle-of-attack range (0° to 32°) but at only two frequencies, 1 and 3.31 cycles per second.

The oscillation-in-yaw tests were made only with the NACA 65A003 airfoil wing at an amplitude of oscillation of ±2° and at the same four frequencies as the oscillation-in-sideslip tests. The angle-of-attack range also was from 0° to 32°.

The static tests were made through the same angle-of-attack range (0° to 32°) at $\beta = 0°$ for lift, drag, and pitching moment and at $\beta = \pm 5°$ for the C_{Y_β}, C_{n_β}, and C_{l_β} terms. At several critical angles of attack the sideslip was varied from -10° to 10° in 2° increments in order to insure that the variation of the lateral stability derivatives was close enough to being linear to satisfactorily permit the use of tests at ±5° to obtain the static derivatives.

Corrections

Jet-boundary corrections to angle of attack and drag coefficient have been determined by the method of reference 8 and are based upon the data obtained from the static sideslip tests at $\beta = 0°$; these corrections have been applied to the steady-state results. No boundary corrections were applied to the oscillation derivatives because they were believed to be small (ref. 9). Blockage corrections determined by the methods presented in reference 10 have been applied to the dynamic pressure and drag. The dynamic data were corrected for the effects of a variation in angularity of the airstream as the model oscillated from side to side in the test section. A correction also was applied to the wind-off oscillation readings for the still-air aerodynamic effect on the model. This correction was obtained by first oscillating the model in free air and then completely enclosing the model and strain gage in a wooden box to shield it from the air. (See fig. 6.) The resonance effect discussed in reference 11 becomes important only for the frequencies considered at Mach numbers near unity and, therefore, requires no consideration for the present investigation. The data have not been

corrected for turbulence or support-strut interference, although the latter may be sizeable at the higher angles of attack.

REDUCTION OF DATA

The equations of motion for a model performing a forced sinusoidal oscillation in sideslip for the yawing moment is

$$\gamma_Z \ddot{y} = M_{Z_{\ddot{y}}} \ddot{y} + M_{Z_{\dot{y}}} \dot{y} + A \sin \omega t + B \cos \omega t \tag{1}$$

and for the rolling moment is

$$\gamma_X \ddot{y} = M_{X_{\ddot{y}}} \ddot{y} + M_{X_{\dot{y}}} \dot{y} + C \sin \omega t + D \cos \omega t \tag{2}$$

where A and C are the maximum in-phase yawing and rolling moments, respectively, and B and D are the corresponding out-of-phase moments supplied by the strain gage. The terms γ_Z and γ_X are used to represent any unbalance of the model about the mounting point that may exist; γ_Z is proportional to the mass and the distance that the center of gravity of the mass is forward or rearward of the mounting point, and γ_X is proportional to the mass and the distance of the mass center of gravity above or below the mounting point. These terms should be small since it was attempted to balance the model about the mounting point. The equations for the displacement, velocity, and acceleration along the Y-axis are given approximately by:

$$y = y_o \sin \omega t$$

$$\dot{y} = y_o \omega \cos \omega t \tag{3}$$

$$\ddot{y} = -y_o \omega^2 \sin \omega t \tag{4}$$

and the resulting expression for the sideslip angle β is:

$$\beta = \frac{y_o \omega \cos \omega t}{V}$$

Substituting equations (3) and (4) into equations (1) and (2), separating the moments that are in phase and out of phase with the motion, and nondimentionalizing give the following expressions:

$$C_{n_\beta} = \frac{-B}{\pi \rho V S_w b_w y_o f} \tag{5}$$

$$C_{l_\beta} = \frac{-D}{\pi\rho V S_w b_w y_{of}} \tag{6}$$

$$C_{n_{\dot\beta}} = \frac{4\gamma_Z}{\rho b_w^2 S_w} + \frac{A}{\pi^2 \rho S_w b_w^2 y_{of}^2} \tag{7}$$

$$C_{l_{\dot\beta}} = \frac{4\gamma_X}{\rho b_w^2 S_w} + \frac{C}{\pi^2 \rho S_w b_w^2 y_{of}^2} \tag{8}$$

Measurements of the moments A, B, C, and D were made with the wind on and off. The wind-off results, wherein the aerodynamic derivatives are zero, measured the γ_Z and γ_X terms and any other deviation from zero that may be present. The aerodynamic derivatives therefore were the differences between the wind-on and wind-off results.

PRESENTATION OF RESULTS

The measured data presented herein are divided into three general groups: (1) the static data for which the longitudinal data are given in figure 7 and the lateral data in figure 8, (2) the oscillation-in-sideslip data for which the aerodynamic derivatives are plotted against angle of attack in figure 9 and against frequency in figure 10, (3) comparison of sharp- and round-nose airfoil data for which the oscillation-in-sideslip data are presented in figure 11 and the oscillation-in-yaw data in figure 12. The computational data for the period and time to damp to one-half amplitude of the oscillatory mode are presented in figures 13 and 14 for altitudes of 0 feet and 50,000 feet, respectively. In addition, the roots of the lateral-stability characteristic equation are presented in tables III and IV for the two altitudes of 0 feet and 50,000 feet. The data of figure 15 are steady-state rolling and yawing data obtained from references 12 and 13 and used in the calculations. A list of the figures and data presented herein is given in table V.

DISCUSSION

Steady-State Tests

The steady-state lift, drag, and pitching-moment coefficients for the three configurations are presented in figure 7. These data are similar to the data presented in reference 12 for the same configurations. The experimental lift-curve slope of the wing through zero angle of

attack is 0.045 compared to a theoretical value of 0.042 and the aerodynamic center is 0.38 compared to a theoretical value of 0.33. Addition of the fuselage and the vertical tail had only minor effects on the static longitudinal characteristics. The steady-state sideslip data (fig. 8) obtained in these tests are similar to the data presented in reference 12 for the same configurations, and the values of the derivatives are generally in good agreement except at the high angles of attack.

The results of the tests in which the sideslip was changed from -10° to 10° for several critical angles of attack indicated that for almost all cases the variation of the derivative was sufficiently linear so that tests at $\beta = \pm 5^\circ$ give a satisfactory representation of the derivative. For the one case in which this was not true, use of the actual slope through $\beta = 0^\circ$ would have resulted in only a minor change in the plot of C_{n_β} against α. Therefore, for the sake of consistency, the slopes between $\beta = \pm 5^\circ$ were used throughout to obtain the static derivatives.

Oscillation-in-Sideslip Tests

In figure 9, the data presented for each configuration show the variation of the four measured derivatives $C_{n_{\dot{\beta},\omega}}$, $C_{l_{\dot{\beta},\omega}}$, $C_{n_{\beta,\omega}}$, and $C_{l_{\beta,\omega}}$ with angle of attack for the different frequencies tested. In figure 10 the variations of the derivatives with frequency for several representative angles of attack are shown. These data show, in general, that (1) the magnitude of the derivatives undergoes very large changes at the high angles of attack, (2) for a given angle of attack the changes in magnitude are dependent upon the frequency of the oscillation, and (3) the variation of the derivatives with angle of attack is more nearly linear for the high-frequency oscillation than for the low-frequency oscillation. This behavior of the oscillatory stability derivatives has been noticed previously (refs. 3, 5, 6, and 14) and has been attributed to the lag in the development of the changes in flow over the wing, which are due to sideslip (ref. 14), and to a lag in the developed sidewash affecting the vertical tail (ref. 15).

The fact that data for the high-frequency oscillations are more nearly linear and at the higher angles of attack are closer to the theoretical results for the wing-alone configuration (refs. 15 and 16) indicates that for high-frequency oscillations the changes in flow that are normally expected for a sideslipping wing do not have sufficient time to develop. However, as the frequency of oscillation is lowered, there is more and more time for breakdown of the flow to occur until the steady-state condition is reached.

Acceleration derivative $C_{n_{\dot{\beta},\omega}}$.- The results for the wing-alone configuration indicate a large increase in $C_{n_{\dot{\beta},\omega}}$ at high angles of attack above approximately 16°, particularly for the lower frequencies (fig. 9(a)). As a matter of fact, this increase in $C_{n_{\dot{\beta},\omega}}$ is responsible, to a large extent, for the large change in the damping term $\left(C_{n_{r,\omega}} - C_{n_{\dot{\beta},\omega}}\right)$ measured by oscillation-in-yaw tests. (See refs. 5 and 14.) Figure 10(a) shows the large change in $C_{n_{\dot{\beta},\omega}}$ as the frequency decreases. The trend of the curves indicates that the largest effects of changes in frequency occur at the low frequencies and that above 3.3 cycles $\left(\frac{\omega b}{2V} = 0.218\right)$ the effects of changes in frequency are less pronounced.

Addition of the fuselage to the wing (figs. 9(b) and 10(b)) resulted in two rather noticeable effects on the oscillation derivatives. First, for comparable angles of attack, it tended to decrease the magnitude of the derivatives somewhat, although they were still large, and second it appeared to delay, until a somewhat higher angle of attack had been attained, the point where the large increases in $C_{n_{\dot{\beta},\omega}}$ became important. The data show that only between the angles of 22° and 30° do these large increases in $C_{n_{\dot{\beta},\omega}}$ occur.

For the wing—fuselage—vertical-tail configuration (figs. 9(c) and 10(c)) there were important changes in $C_{n_{\dot{\beta},\omega}}$ with changes in frequency throughout the angle-of-attack range; whereas, for the previous configurations these changes occurred only at the higher angle-of-attack range. It is interesting to note that at the low angles of attack an increase in the frequency of motion results in a decrease in $C_{n_{\dot{\beta},\omega}}$. As a matter of fact, the magnitude of the negative values of $C_{n_{\dot{\beta},\omega}}$ at any but the lowest frequency is of the same order as the steady-state damping $\left(-C_{n_r}\right)$ shown in figure 15 for this configuration. This would indicate that, unless the oscillatory-damping-in-yaw $\left(-C_{n_{r,\omega}}\right)$ term increases with frequency, a configuration such as this would have little or no damping in yaw during lateral oscillatory motions at low angles of attack for high frequencies of oscillation. At the high angles of attack, above 30°, the vertical tail tended to help maintain the value of $C_{n_{\dot{\beta},\omega}}$ large, rather than permit a decrease as occurred for the wing-fuselage combination.

Acceleration derivative $C_{l_{\dot{\beta},\omega}}$.- The $C_{l_{\dot{\beta},\omega}}$ data for the wing-alone configuration (figs. 9(a) and 10(a)) exhibit characteristics similar to those for $C_{n_{\dot{\beta},\omega}}$ in that at the higher angles of attack there are large increases in magnitude of $C_{l_{\dot{\beta},\omega}}$ and these increases are dependent on the frequency of motion. The slower the oscillation, the larger the magnitude of $C_{l_{\dot{\beta},\omega}}$.

The addition of the fuselage or of the fuselage and vertical tail (figs. 9(b), 9(c), 10(b), and 10(c)) resulted in a smaller increase in magnitude of $C_{l_{\dot{\beta},\omega}}$ at the higher angles of attack than was obtained for the wing alone and also tended to delay until a higher angle of attack was attained the point where these sharp increases in magnitude take place.

Directional stability $C_{n_{\beta,\omega}}$.- The directional-stability data for the wing alone presented in figures 9(a) and 10(a) show that at low angles of attack the oscillatory and steady-state values are about the same and both agree well with theoretical values. (Theoretical values were obtained by methods presented in ref. 16.) In the high-angle-of-attack range where the values for the steady-state directional stability decreased and became negative, the oscillatory values remained considerably higher. This increase in stability became larger as the frequency of motion increased so that at the higher frequencies the oscillatory values of $C_{n_{\beta,\omega}}$ were closer to theoretical values than to the steady-state values.

The data for the wing-fuselage combination (figs. 9(b) and 10(b)) show an effect due to frequency of the oscillatory motion which was similar to that of the wing alone. The entire group of data, however, was displaced in a negative direction (decreased directional stability) by an increment in $C_{n_{\beta}}$ of about 0.05.

For the wing—fuselage—vertical-tail configuration in the low-angle-of-attack range (fig. 9(c)), the steady-state stability is much higher than that for the previous two configurations because of the presence of the vertical tail. The oscillatory results show a considerable increase over the steady-state values. This increased stability shown by the oscillatory tests is maintained throughout the angle-of-attack range so that at the higher angles where the static stability falls to zero and becomes negative the oscillatory test values maintain stability to a considerably higher angle of attack. Figure 10(c) shows the rapid rise that occurs for $C_{n_{\beta,\omega}}$ as the frequency of motion is

increased from zero to about $\frac{\omega b}{2V} = 0.1$. Above $\frac{\omega b}{2V} = 0.1$ the values of $C_{n_{\beta,\omega}}$ tend to level off and then decrease slightly.

Effective dihedral parameter $-C_{l_\beta}$.- The effective dihedral-parameter $\left(-C_{l_\beta}\right)$ results for the wing alone (fig. 9(a)) were, in general, somewhat similar to the C_{n_β} results. At the lower angles of attack the static and oscillatory results are similar and approximately the same as the theoretical values. The theoretical values were obtained by the methods presented in reference 17 in which the effects of taper are omitted. At the higher angles of attack the static effective dihedral decreases and becomes negative, whereas, the oscillatory values remain higher. Increasing the frequency of oscillation at the high angles increased the dihedral effect so that it more nearly approached the theoretical value.

Addition of the fuselage to the wing (figs. 9(b) and 10(b)) did not appreciably affect the oscillatory data. It did however cause an appreciable increase in the static test value of effective dihedral at the high angles of attack so that this value is among the oscillation test values. The fuselage apparently prevents the development of the large disparity of separation effects that occurred on the leading and trailing panels for the wing alone. In this respect, the effect of the fuselage is somewhat similar to the results of the oscillation tests in which the full-separation effect does not have sufficient time to develop.

The results for the wing—fuselage—vertical-tail configuration (figs. 9(c) and 10(c)) are very similar to those for the wing-fuselage configuration.

Comparison of Oscillation Data for Delta Wings with a Round Leading Edge and a Relatively Sharp Leading Edge

The large changes in the oscillation derivatives that were obtained at the higher angles of attack have been attributed to the effects of flow separation. In order to pursue this idea a little further, some tests were made on another wing of the same plan form and approximate thickness but with a flat-plate airfoil section and a much larger leading-edge radius. A comparison is made of the results for both wings from oscillation-in-sideslip tests and oscillation-in-yaw tests in figures 11 and 12, respectively. It can be seen that for both cases changes in frequency of motion cause much larger changes in magnitude of the derivatives for the sharp-nose airfoil than for the

round-nose airfoil. These results substantiate the idea that the large frequency effects are closely associated with the separation of flow over the wing inasmuch as it is well known that separation is likely to occur somewhat earlier and usually is more pronounced for a sharp leading edge than for a well rounded one.

Effect of Sideslip Oscillatory Derivatives on Period and Time To Damp to One-Half Amplitude

In order to determine the effect that the sideslip oscillatory derivatives may have on the calculated stability of a typical delta-wing airplane, some computations of the period and time to damp to one-half amplitude were made. In these computations, both the oscillatory stability derivatives discussed herein and the steady-state derivatives shown in figure 15 were used. The calculations were made for two altitudes, 0 and 50,000 feet, and at angles of attack from 2° to 28°. For the oscillatory cases, P and $T_{1/2}$ were obtained by a process of iteration. Initially, the values for the sideslip derivatives for some assumed frequency were inserted into the equations of motion presented in reference 4, and the period was calculated. The computed period usually differed from that initially assumed and, therefore, new values of the derivatives for a period or frequency close to the computed period were used. This process was continued until the period for which the derivatives were used agreed with period resulting from the calculations. This procedure is normally not necessary where there is little change of the derivatives with frequency. The time to damp is shown only for the oscillatory mode of motion in figures 13 and 14 because it is believed that the stability derivatives obtained from oscillation tests, such as these, are most pertinent for the oscillatory mode. All four roots of the lateral-stability characteristic equation are given in tables III and IV.

Figures 13 and 14 show that there is a considerable difference in the time to damp which depends upon whether the steady-state or oscillatory derivatives are used. At zero altitude, for instance, the time to damp to one-half amplitude for the low-angle-of-attack region is longer if the oscillatory derivatives are used. This probably occurs because of a decrease in the damping as a result of the more negative value of $C_{n_{\dot{\beta},\omega}}$ discussed previously. At the higher angles of attack where the damping was larger, no oscillatory mode is indicated. The period of the oscillation was practically unaffected at the low angles of attack. At the higher angles of attack, however, the period appeared to be considerably affected.

The computations for an altitude of 50,000 feet indicate results similar to those for the lower altitude, except that the indicated damping using the oscillatory derivatives is greater even at moderate angles of attack.

CONCLUSIONS

The results of tests made to determine the effects of frequency of oscillation in sideslip at a maximum amplitude of $\pm 2^{\circ}$ on the stability derivatives of a typical 60° delta-wing airplane configuration indicate the following conclusions:

1. For all three configurations tested (wing alone, wing-fuselage combination, and wing—fuselage—vertical-tail combination), the magnitude of the oscillatory sideslipping derivatives underwent very large changes at the high angles of attack and the magnitude of the changes was dependent upon the frequency of oscillation. In general at the low angles of attack little effect of frequency on the oscillatory derivative was noted, with the exception of the yawing-moment derivatives of the complete-model configuration for which a relatively large effect of frequency was noted.

2. For the complete-model configuration (wing-fuselage and vertical tail) the oscillatory motion introduced a considerable effect on both the oscillatory yawing-moment-acceleration derivative $C_{n_{\dot{\beta}},\omega}$ and the oscillatory directional-stability derivative $C_{n_{\beta},\omega}$ throughout the angle-of-attack range. In the low-angle-of-attack range, $C_{n_{\dot{\beta}},\omega}$ became increasingly negative with frequency so that at a reduced frequency of about 0.218 the negative value of $C_{n_{\dot{\beta}},\omega}$ was equal to the steady-state damping in yaw. At high angles of attack $C_{n_{\dot{\beta}},\omega}$ went to very large positive values. The oscillatory directional stability was greater than the steady-state directional stability throughout the angle-of-attack range.

3. For the complete-model configuration the effects of frequency of motion on the rolling-moment derivatives were relatively small at the low angles of attack and were large at the high angles of attack.

4. The oscillatory rolling-moment-acceleration derivative $C_{l_{\dot{\beta}},\omega}$ and the derivative $C_{n_{\dot{\beta}},\omega}$ for the wing-alone configuration generally increased in magnitude as the frequency of oscillation decreased. The

oscillatory sideslipping derivatives (both rolling moment and yawing moment) $C_{l_{\beta,\omega}}$ and $C_{n_{\beta,\omega}}$ deviated further from the static derivative and at the high angles of attack more closely approached the theoretical values as the frequency of oscillation increased.

5. Addition of a fuselage to the wing delayed, until higher angles of attack, the large changes in the oscillatory stability derivatives, and although this addition tended to decrease the effect of frequency changes on the derivatives somewhat, the magnitude was still large.

6. Leading-edge radius had a very pronounced effect on the oscillatory stability derivatives for the wing-alone configuration. Decreasing the leading-edge radius (sharper nose) increased the magnitude of the frequency effects obtained for oscillations in both sideslip and yaw.

7. Comparison of the calculated period of oscillation and time to damp to one-half amplitude for a typical delta-wing airplane using steady-state data and oscillatory data where applicable shows that at low angles of attack the period is unaffected, whereas, the time to damp to one-half amplitude is increased by using the oscillatory derivatives. At high angles of attack, however, use of the oscillatory data in the computation of the roots of the lateral-stability characteristic equation indicated more damping and stability than obtained by using the steady-state data. Generally the data for an altitude of 50,000 feet indicated similar characteristics, but with an improvement even at moderate angles of attack.

Langley Aeronautical Laboratory,
National Advisory Committee for Aeronautics,
Langley Field, Va., May 24, 1957.

REFERENCES

1. Bird, John D., Jaquet, Byron M., and Cowan, John W.: Effect of Fuselage and Tail Surfaces on Low-Speed Yawing Characteristics of a Swept-Wing Model As Determined in Curved-Flow Test Section of Langley Stability Tunnel. NACA TN 2483, 1951. (Supersedes NACA RM L8G13.)

2. Beam, Benjamin H., Reed, Verlin D., and Lopez, Armando E.: Wind-Tunnel Measurements at Subsonic Speeds of the Static and Dynamic-Rotary Stability Derivatives of a Triangular-Wing Airplane Model Having a Triangular Vertical Tail. NACA RM A55A28, 1955.

3. Riley, Donald R., Bird, John D., and Fisher, Lewis R.: Experimental Determination of the Aerodynamic Derivatives Arising From Acceleration in Sideslip for a Triangular, a Swept, and an Unswept Wing. NACA RM L55A07, 1955.

4. Campbell, John P., and Woodling, Carroll H.: Calculated Effects of the Lateral Acceleration Derivatives on the Dynamic Lateral Stability of a Delta-Wing Airplane. NACA RM L54K26, 1955.

5. Fisher, Lewis R.: Experimental Determination of the Effects of Frequency and Amplitude on the Lateral Stability Derivatives for a Delta, a Swept, and an Unswept Wing Oscillating in Yaw. NACA RM L56A19, 1956.

6. Queijo, M. J., Fletcher, Herman S., Marple, C. G., and Hughes, F. M.: Preliminary Measurements of the Aerodynamic Yawing Derivatives of a Triangular, a Swept, and an Unswept Wing Performing Pure Yawing Oscillations, With a Description of the Instrumentation Employed. NACA RM L55L14, 1956.

7. Sternfield, Leonard, and Gates, Ordway B., Jr.: A Simplified Method for the Determination and Analysis of the Neutral-Lateral-Oscillatory-Stability Boundary. NACA Rep. 943, 1949. (Supersedes NACA TN 1727.)

8. Silverstein, Abe, and White, James A.: Wind-Tunnel Interference With Particular Reference to Off-Center Positions of the Wing and to the Downwash at the Tail. NACA Rep. 547, 1936.

9. Evans, J. M.: Stability Derivatives. Wind Tunnel Interference on the Lateral Derivatives l_p, l_r and l_v With Particular Reference to l_p. Rep. ACA-33, Australian Council for Aeronautics, Mar. 1947.

10. Herriot, John G.: Blockage Corrections for Three-Dimensional-Flow Closed-Throat Wind Tunnels, With Consideration of the Effect of Compressibility. NACA Rep. 995, 1950. (Supersedes NACA RM A7B28.)

11. Runyan, Harry L., Woolston, Donald S., and Rainey, A. Gerald: Theoretical and Experimental Investigation of the Effect of Tunnel Walls on the Forces on an Oscillating Airfoil in Two-Dimensional Subsonic Compressible Flow. NACA Rep. 1262, 1956. (Supersedes NACA TN 3416.)

12. Goodman, Alex, and Thomas, David F., Jr.: Effects of Wing Position and Fuselage Size on the Low-Speed Static and Rolling Stability Characteristics of a Delta-Wing Model. NACA Rep. 1224, 1955. (Supersedes NACA TN 3063.)

13. Jaquet, Byron M., and Fletcher, Herman S.: Experimental Steady-State Yawing Derivatives of a 60° Delta-Wing Model as Affected by Changes in Vertical Position of the Wing and in Ratio of Fuselage Diameter to Wing Span. NACA TN 3843, 1956.

14. Campbell, John P., Johnson, Joseph L., Jr., and Hewes, Donald E.: Low-Speed Study of the Effect of Frequency on the Stability Derivatives of Wings Oscillating in Yaw With Particular Reference to High Angle-of-Attack Conditions. NACA RM L55H05, 1955.

15. Fisher, Lewis R., and Fletcher, Herman S.: Effect of Lag of Sidewash on the Vertical-Tail Contribution to Oscillatory Damping in Yaw of Airplane Models. NACA TN 3356, 1955.

16. Toll, Thomas A., and Queijo, M. J.: Approximate Relations and Charts for Low-Speed Stability Derivatives of Swept Wings. NACA TN 1581, 1948.

17. Queijo, M. J.: Theoretical Span Load Distributions and Rolling Moments for Sideslipping Wings of Arbitrary Plan Form in Incompressible Flow. NACA Rep. 1269, 1956. (Supersedes NACA TN 3605.)

TABLE I.- PERTINENT GEOMETRIC CHARACTERISTICS OF MODELS

Fuselage:	
Length, in.	54.0
Maximum diameter, d, in.	6.0
Fineness ratio	9.0
Body-size ratio, d/b_W	0.165
Volume, cu in.	990
Side area, sq in.	252
Wing:	
Aspect ratio	2.31
Taper ratio	0
Leading-edge sweep angle, deg	60
Dihedral angle, deg	0
Twist, deg	0
NACA airfoil section	65A003
Area, sq in.	576.7
Span, in.	36.5
Mean aerodynamic chord, in.	21.1
Root chord, in.	31.6
Vertical tail:	
Aspect ratio	2.18
Taper ratio	0
Leading-edge sweep angle, deg	42.5
NACA airfoil section	65-006
Area, sq in.	66.0
Span, in.	12.00
Root chord, in.	11.00
Mean aerodynamic chord, in.	7.35
Tail length, in.	21.5
Area ratio, S_V/S_W	0.115
Tail-length ratio, l_V/b_W	0.59

TABLE II.- ORDINATES FOR NACA 65A003 AND 65-006 AIRFOILS AND FOR THE FUSELAGE

[Station and ordinates for wing and vertical tail in percent airfoil chord; station and ordinates for fuselage in percent of fuselage length]

Wing	
NACA 65A003	
Station	Ordinate
0	0
.50	.234
.75	.284
1.25	.362
2.50	.493
5.00	.658
7.50	.796
10.00	.912
15.00	1.097
20.00	1.236
25.00	1.342
30.00	1.420
35.00	1.472
40.00	1.498
45.00	1.497
50.00	1.465
55.00	1.402
60.00	1.309
65.00	1.191
70.00	1.053
75.00	.897
80.00	.727
85.00	.549
90.00	.369
95.00	.188
100.00	.007
L. E. radius, 0.057	

Vertical tail	
NACA 65-006	
Station	Ordinate
0	0
.50	.476
.75	.574
1.25	.717
2.50	.956
5.00	1.310
7.50	1.589
10.00	1.824
15.00	2.197
20.00	2.482
25.00	2.697
30.00	2.852
35.00	2.952
40.00	2.998
45.00	2.983
50.00	2.900
55.00	2.741
60.00	2.518
65.00	2.246
70.00	1.935
75.00	1.594
80.00	1.233
85.00	.865
90.00	.510
95.00	.195
100.00	0
L. E. radius, 0.240	

Fuselage	
Station	Ordinate
0	0
.6	.17
.9	.24
1.5	.41
3.0	.80
6.0	1.54
9.0	2.22
12.0	2.84
18.0	3.87
24.0	4.67
30.0	5.20
36.0	5.50
40.0	5.56
42.0	5.54
48.0	5.52
54.0	5.41
60.0	5.24
66.0	5.04
72.0	4.76
78.0	4.43
84.0	4.06
90.0	3.61
96.0	3.13
100.0	2.76

TABLE III.- ROOTS OF THE LATERAL-STABILITY CHARACTERISTIC EQUATION

[Altitude, 0 ft; μ = 11.85; b = 39.1 ft]

α, deg	V, ft/sec	Steady state				Oscillatory			
		1	2	3	4	1	2	3	4
2	701	-0.0124	-2.875	-0.6197 + 3.549i	-0.6197 - 3.549i	-0.0086	-2.892	-0.3018 + 3.946i	-0.3018 - 3.946i
10	289	-.1269	-2.479	-.8095 + 4.662i	-.8095 - 4.662i	-.0824	-2.574	-.2258 + 5.021i	-.2258 - 5.021i
16	223	-.1689	-2.463	-.8814 + 5.288i	-.8814 - 5.288i	-.1478	-2.533	-.5202 + 5.833i	-.5202 - 5.833i
20	201	-.2094	-2.419	-.8755 + 5.409i	-.8755 + 5.409i	-.2180	-2.432	-.7951 + 6.598i	-.7951 - 6.598i
22	192.9	-.2290	-2.573	-.9339 + 4.952i	-.9339 - 4.952i	-.2552	-2.480	-.4752 + 6.622i	-.4752 - 6.622i
24	187.0	-.2836	-2.687	-.8855 + 3.614i	-.8855 - 3.614i	-.2865	-2.484	-.6556 + 6.504i	-.6556 - 6.504i
26	181.6	.3850 + 0.4678i	.3850 - 0.4678i	-2.788 + 1.284i	-2.788 - 1.284i	-.4049	-.5159	-1.752	-21.78
28	178	-.0535	2.311	-3.602 + 1.628i	-3.602 - 1.628i	-.0014	.0150	-1.862	-37.88

TABLE IV.- ROOTS OF THE LATERAL-STABILITY CHARACTERISTIC EQUATION

[Altitude, 50,000 ft; μ = 77.8; b = 39.1 ft]

α, deg	V, ft/sec	Steady state				Oscillatory			
		1	2	3	4	1	2	3	4
10	724.0	-0.1317	-2.432	-0.8306 + 12.26i	-0.8306 - 12.26i	-0.0707	-2.557	-0.5657 + 12.98i	-0.5657 - 12.98i
16	561.0	-.1688	-2.410	-.9076 + 13.86i	-.9076 - 13.86i	-.1033	-2.527	-1.105 + 15.34i	-1.105 - 15.34i
20	508.0	-.2092	-2.375	-.8976 + 14.15i	-.8976 - 14.15i	-.1513	-2.473	-1.518 + 16.04i	-1.518 - 16.04i
22	490.3	-.2331	-2.490	-.9732 + 13.13i	-.9732 - 13.13i	-.1723	-2.630	-1.778 + 15.98i	-1.778 - 15.98i
24	475.6	-.2849	-2.447	-1.005 + 9.995i	-1.005 - 9.995i	-.1919	-2.765	-2.921 + 15.37i	-2.921 - 15.37i
26	462.6	.8249 + 0.4716i	.8249 - 0.4716i	-3.228 + 3.886i	-3.228 - 3.886i	-.0436 + 0.6048i	-.0436 - 0.6048i	-3.133	-23.88
28	453.0	-.0531	6.010	-5.452 + 3.167i	-5.452 - 3.167i	-.0351	1.540	-3.009	-39.40

TABLE V.- LIST OF TESTS AND DATA FIGURES

Configuration	Data	Oscillatory amplitude of sideslip	Figure
Wing Wing-fuselage Wing-fuselage-tail	Steady-state C_L, C_m, and C_D against α		7
Wing Wing-fuselage Wing-fuselage-tail	Steady-state C_{n_β}, C_{l_β}, and C_{Y_β} against α		8
Wing Wing-fuselage Wing-fuselage-tail	$C_{n_{\dot\beta,\omega}}$, $C_{l_{\dot\beta,\omega}}$, $C_{n_{\beta,\omega}}$, and $C_{l_{\beta,\omega}}$ against α	$\pm 2^\circ$	9(a) 9(b) 9(c)
Wing Wing-fuselage Wing-fuselage-tail	$C_{n_{\dot\beta,\omega}}$, $C_{l_{\dot\beta,\omega}}$, $C_{n_{\beta,\omega}}$, and $C_{l_{\beta,\omega}}$ against $\frac{\omega b}{2V}$	$\pm 2^\circ$	10(a) 10(b) 10(c)
Airfoil wing Flat-plate wing	$C_{n_{\dot\beta,\omega}}$, $C_{l_{\dot\beta,\omega}}$, $C_{n_{\beta,\omega}}$, and $C_{l_{\beta,\omega}}$ against α	$\pm 2^\circ$	11
Airfoil wing Flat-plate wing	$C_{n_{r,\omega}} - C_{n_{\dot\beta,\omega}}$, $C_{l_{r,\omega}} - C_{l_{\dot\beta,\omega}}$, $C_{n_{\beta,\omega}} + \left(\frac{\omega b}{2V}\right)^2 C_{n_{\dot r,\omega}}$, and $C_{l_{\beta,\omega}} + \left(\frac{\omega b}{2V}\right)^2 C_{l_{\dot r,\omega}}$ against α	$\pm 2^\circ$	12
Wing-fuselage-tail	P, $T_{1/2}$, and T_2 against α for 0-foot altitude P, $T_{1/2}$, and T_2 against α for 50,000-foot altitude		13 14
Wing-fuselage-tail	Steady-state C_{l_r}, C_{n_r}, C_{Y_r}, C_{l_p}, C_{n_p}, and C_{Y_p} against α		15

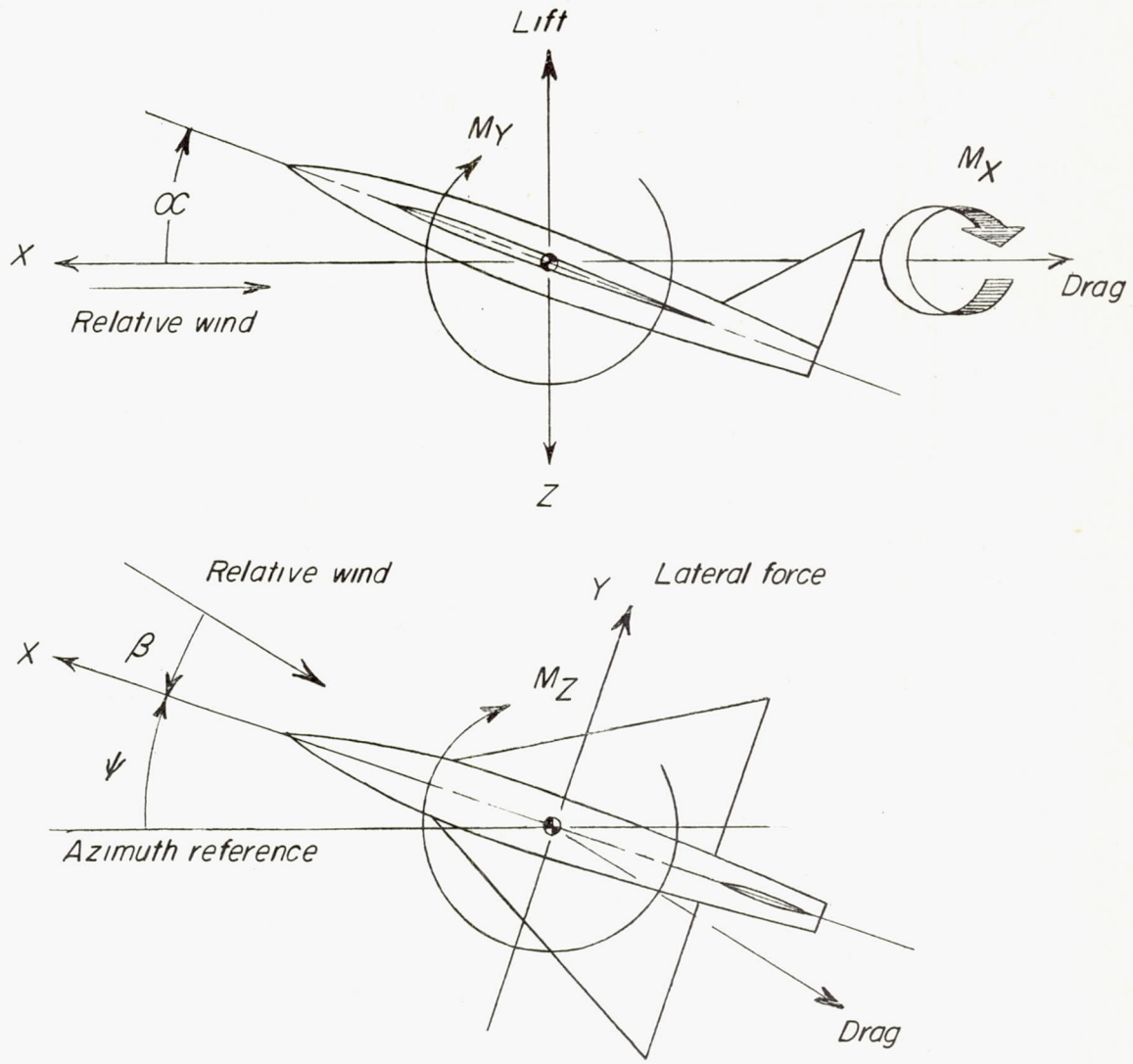

Figure 1.- System of stability axes. Arrows indicate positive forces, moments, and angular displacements.

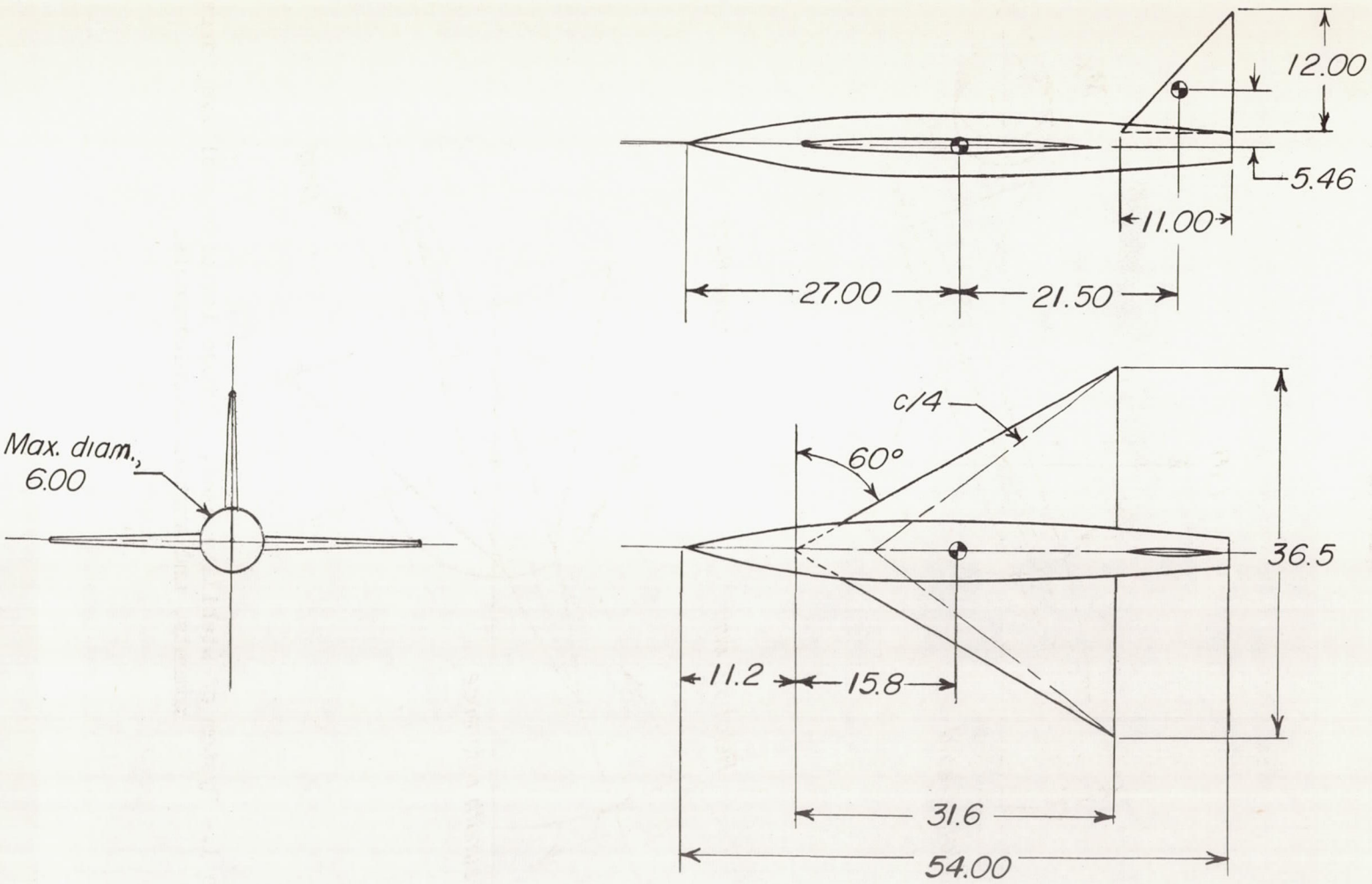

Figure 2.- Three-view sketch of model used in tests. (All dimensions are in inches.)

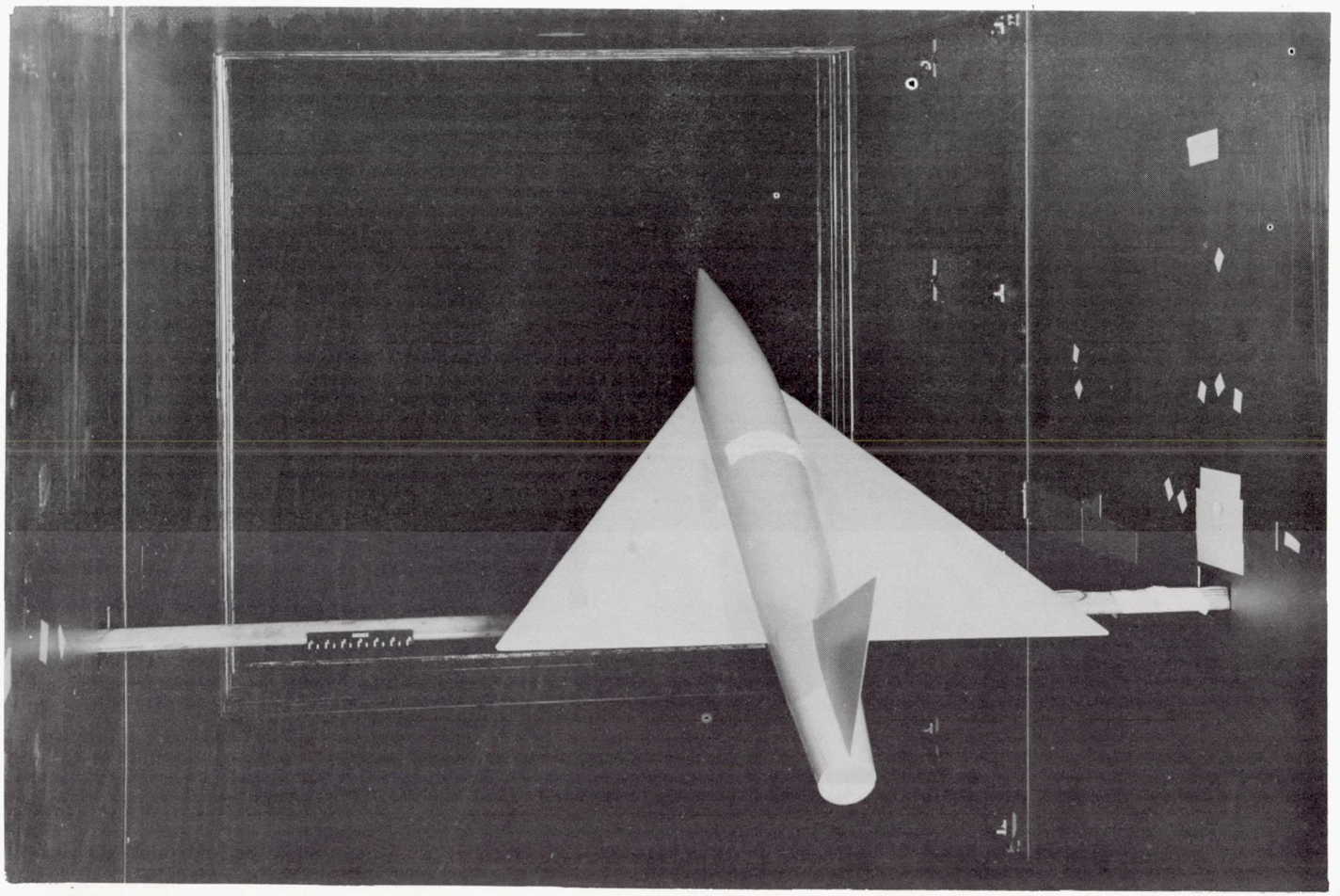

L-90781

Figure 3.- Photograph of the complete-model configuration mounted in the 6- by 6-foot test section of the Langley stability tunnel for oscillation-in-sideslip tests.

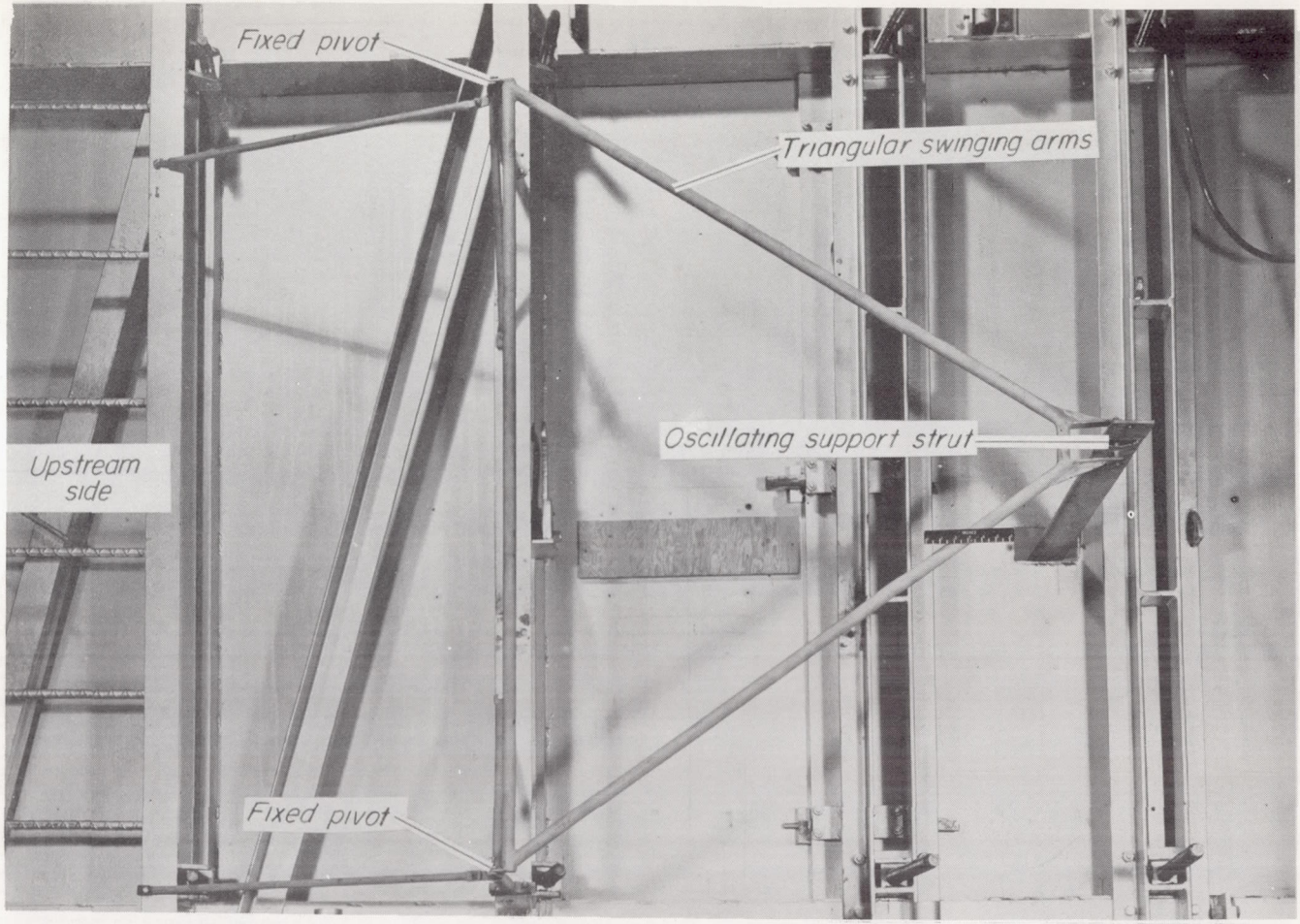

(a) View of left side of tunnel. L-92023.1

Figure 4.- Photographs showing the oscillation apparatus and drive mechanism.

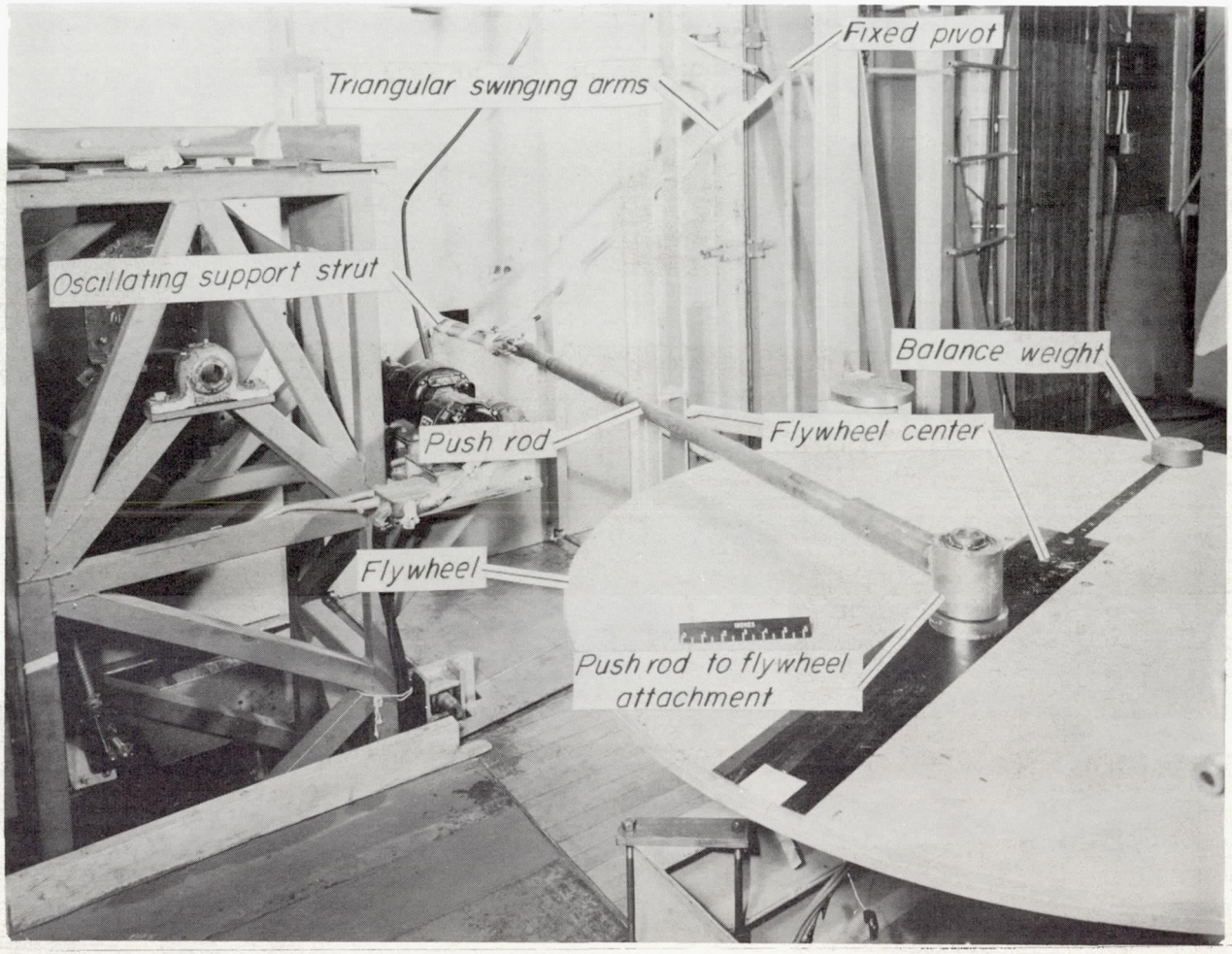

(b) View of right side of tunnel. L-90775.1

Figure 4.- Continued.

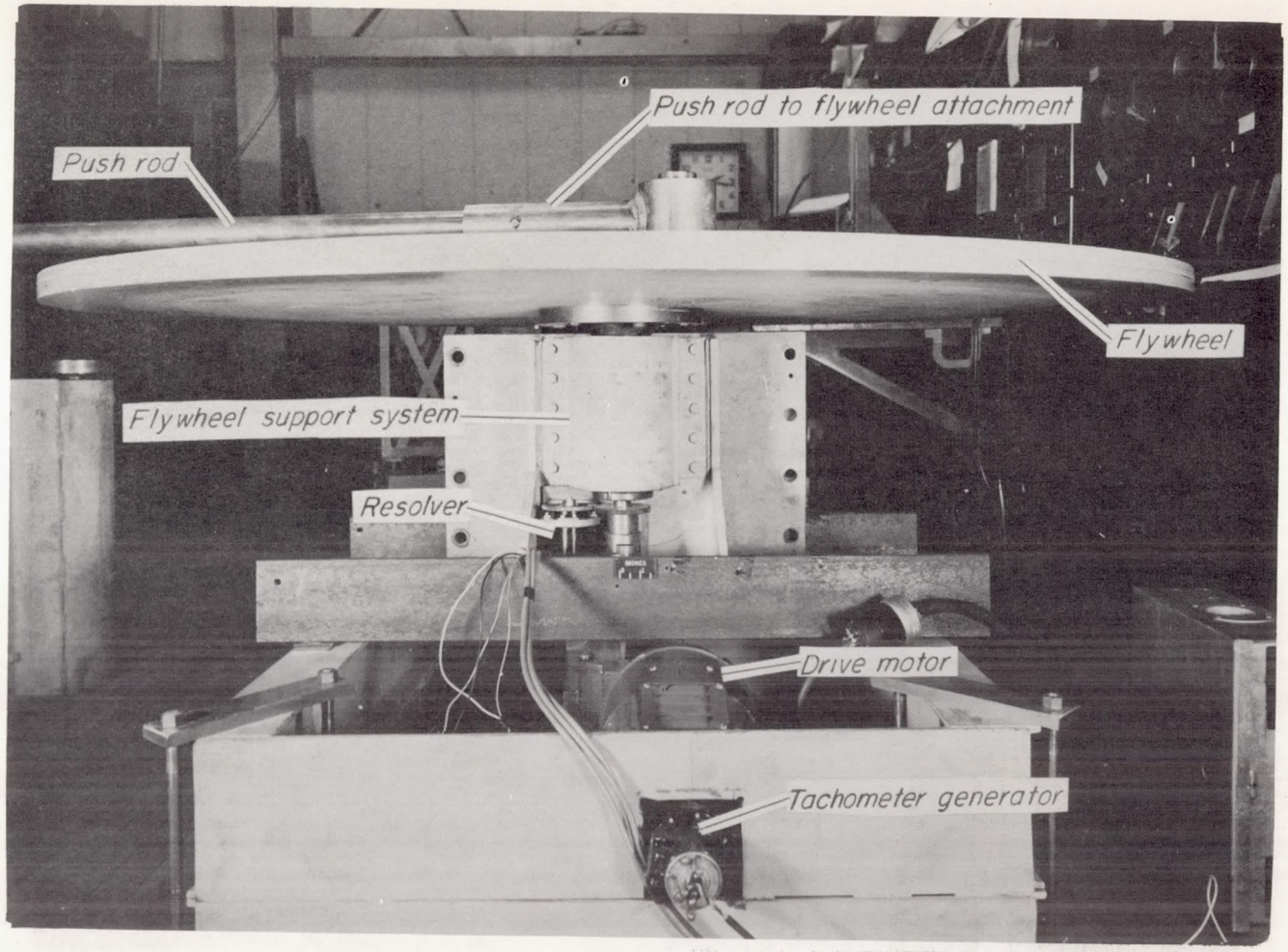

(c) View of the drive mechanism. L-90776.1

Figure 4.- Concluded.

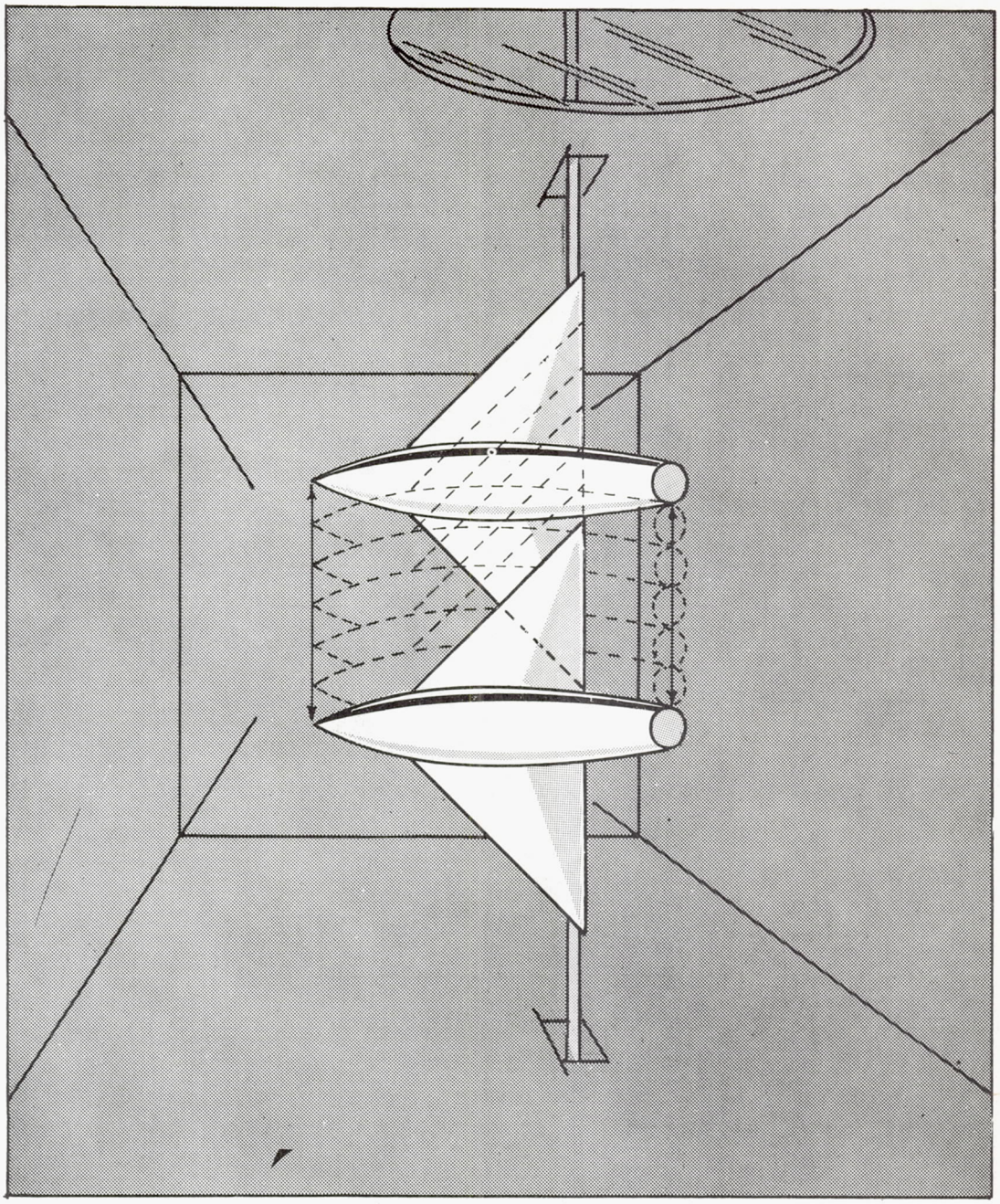

Figure 5.- Sketch showing typical model motion in the tunnel.

L-90778

Figure 6.- Photograph of the box used to encase the model for determining the still-air correction.

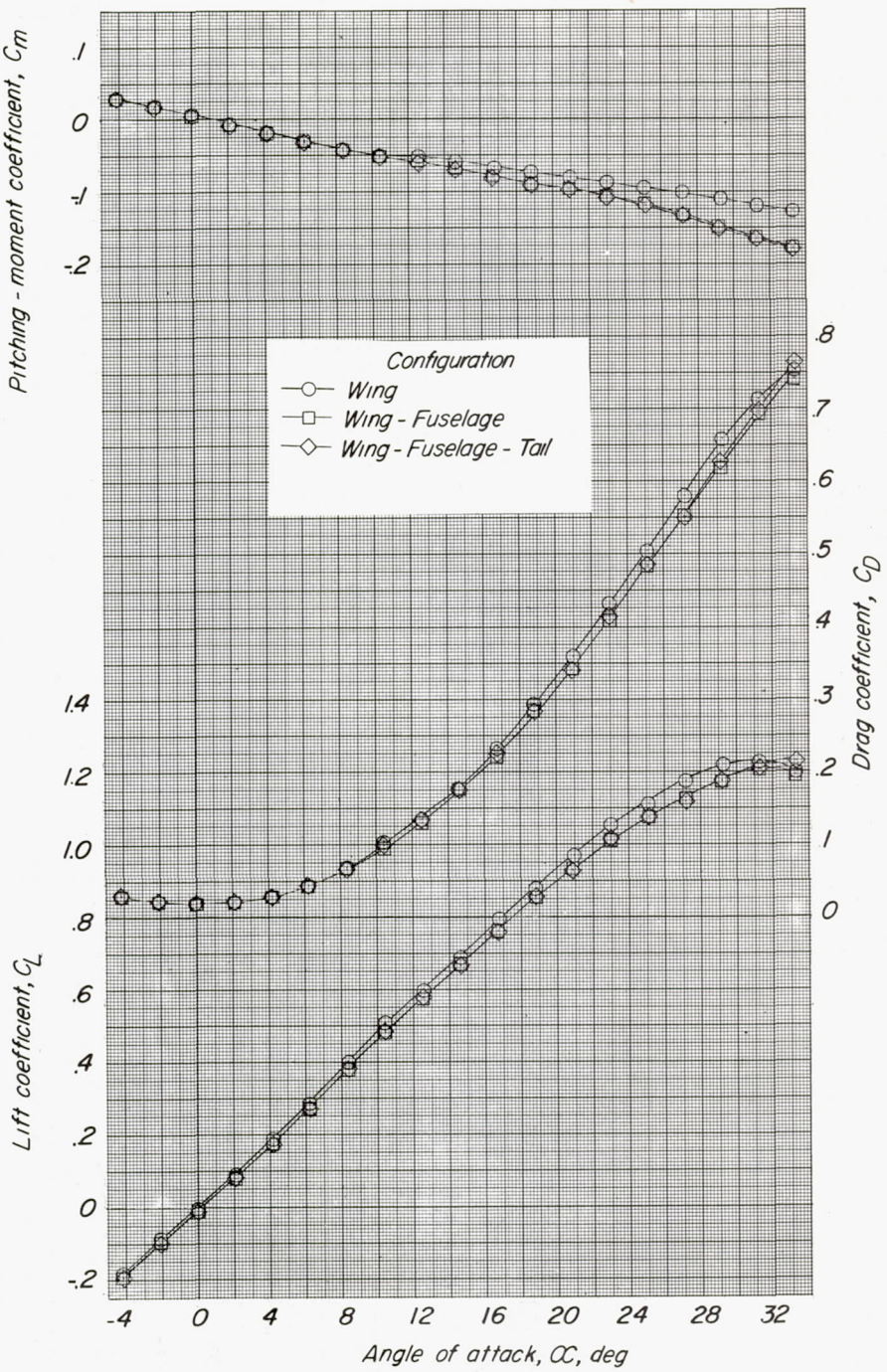

Figure 7.- Variation of static lift, drag, and pitching-moment coefficients with angle of attack for the three configurations tested. $\beta = 0$.

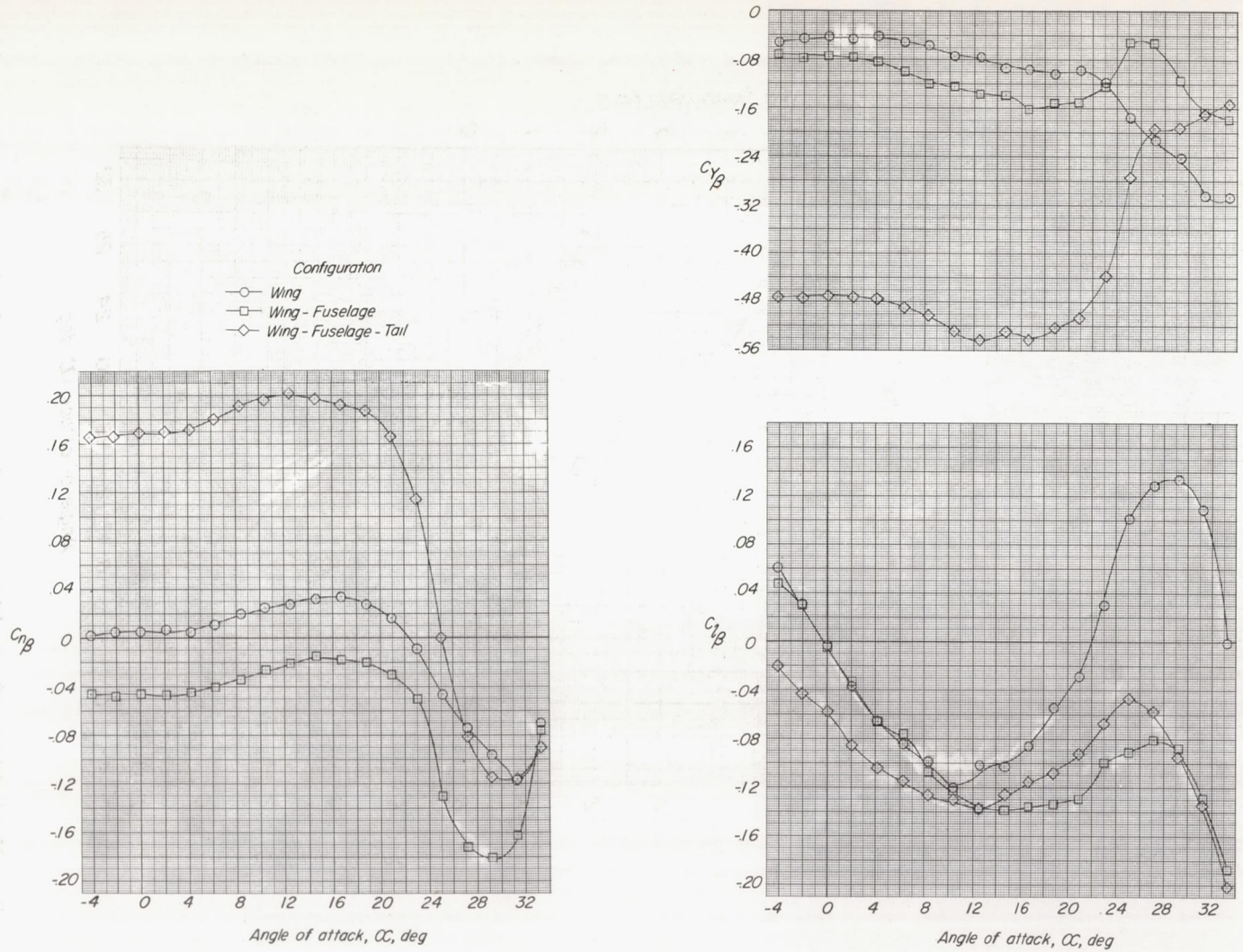

Figure 8.- Variation of the static lateral stability characteristics with angle of attack for three configurations tested.

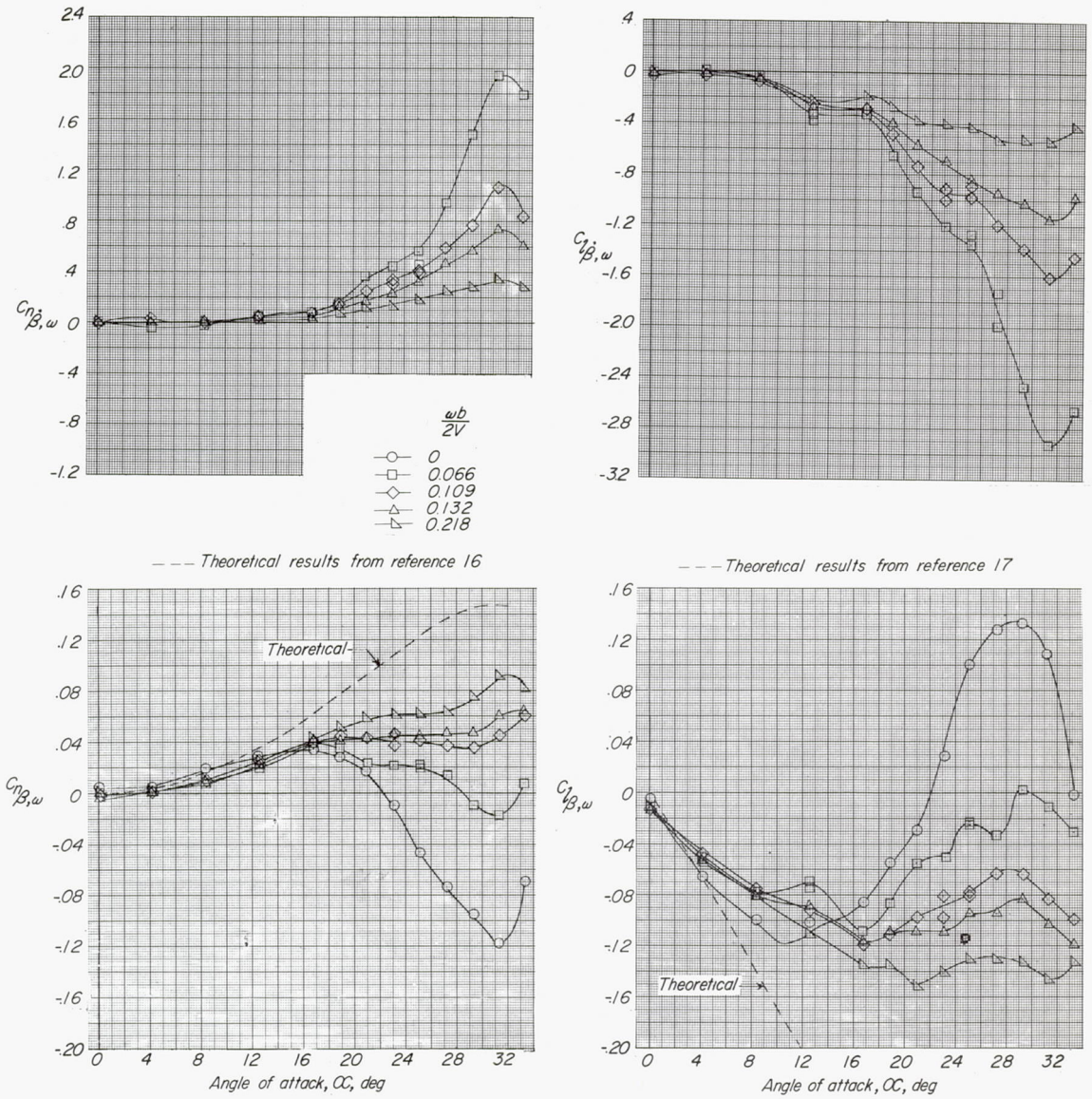

(a) Wing-alone configuration.

Figure 9.- Variation of stability derivatives with angles of attack measured during oscillation for the three configurations tested.

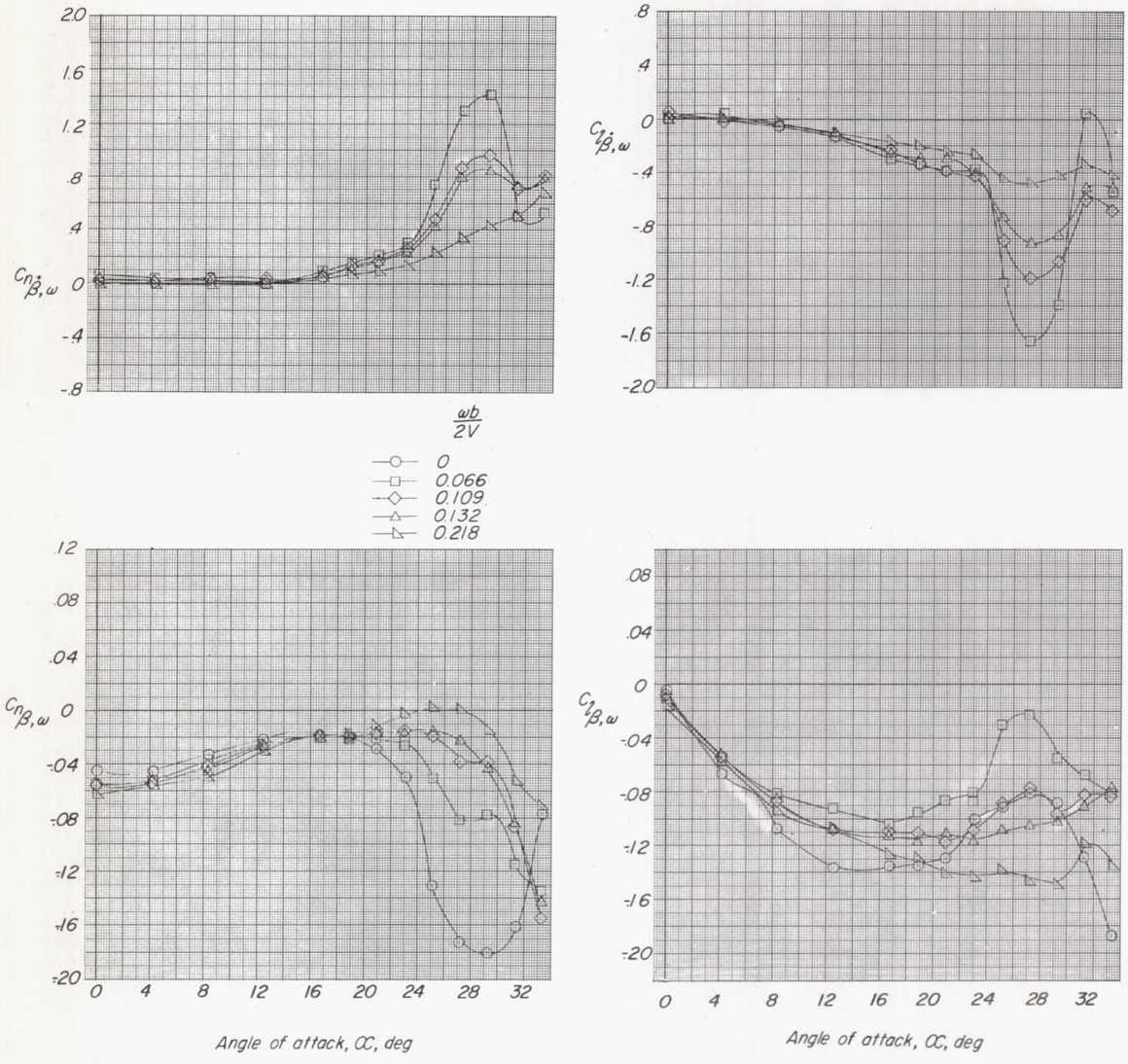

(b) Wing-fuselage configuration.

Figure 9.- Continued.

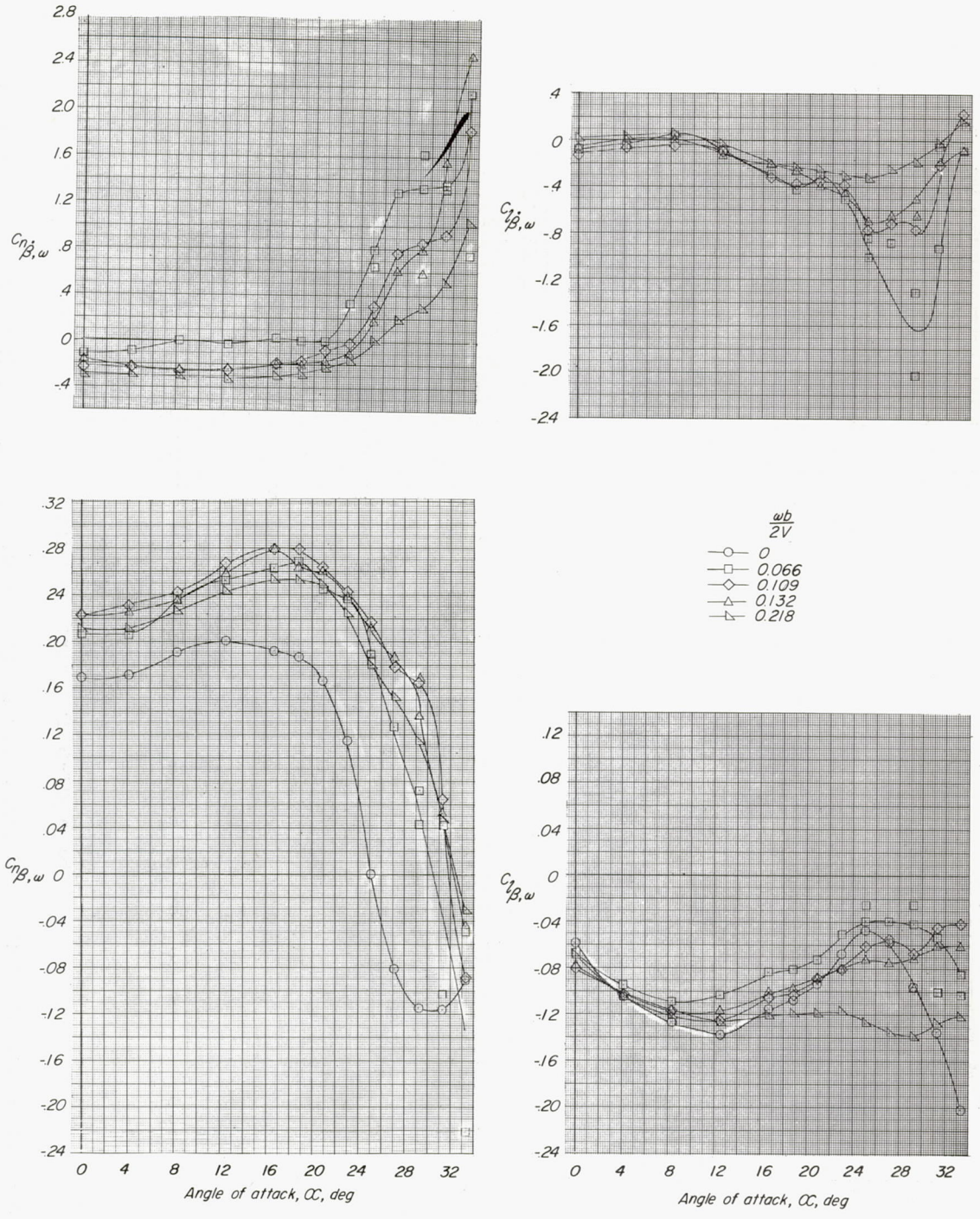

(c) Wing-fuselage-tail configuration.

Figure 9.- Concluded.

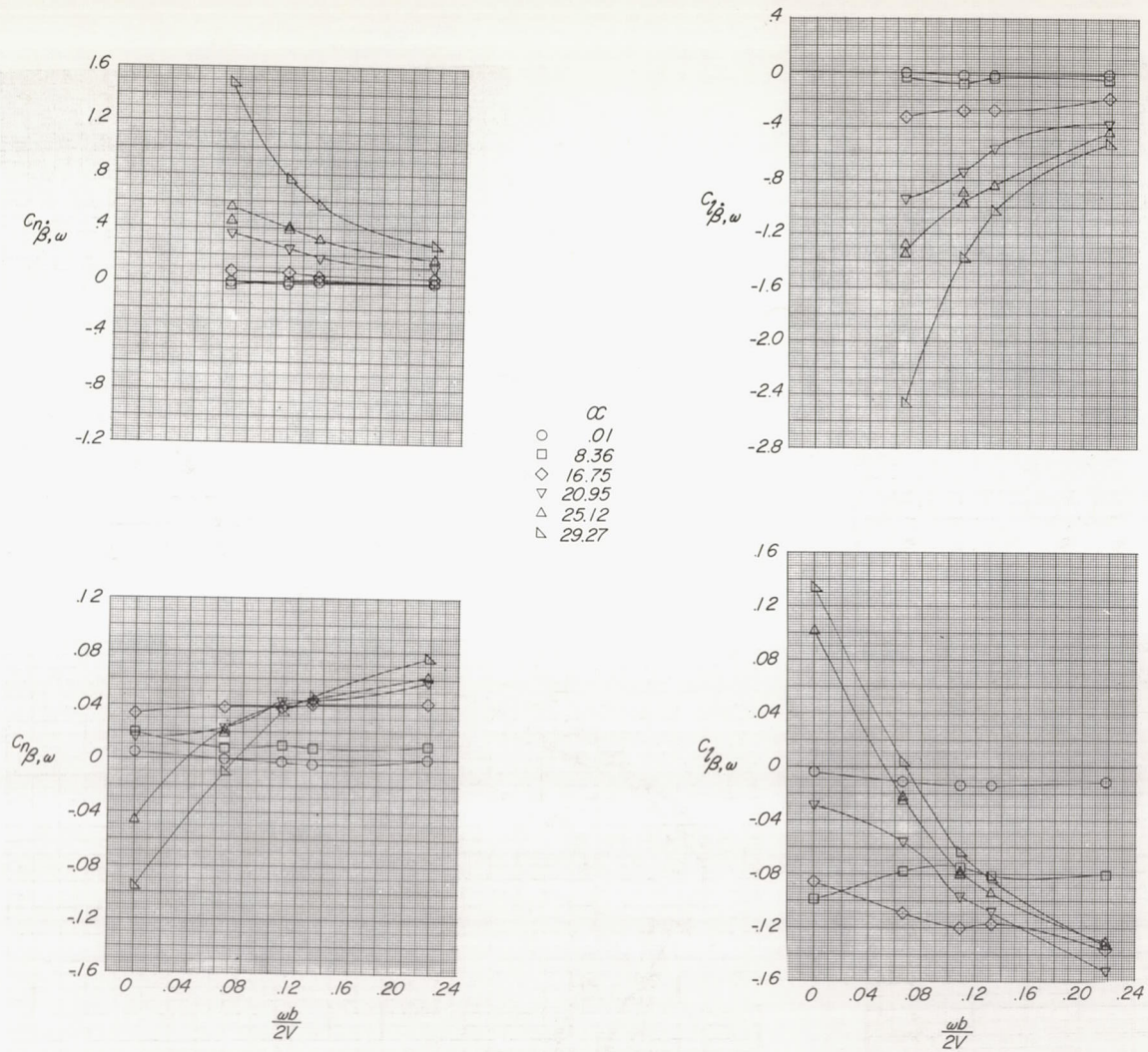

(a) Wing-alone configuration.

Figure 10.- Variation of stability derivatives with frequency for various angles of attack for the three configurations tested.

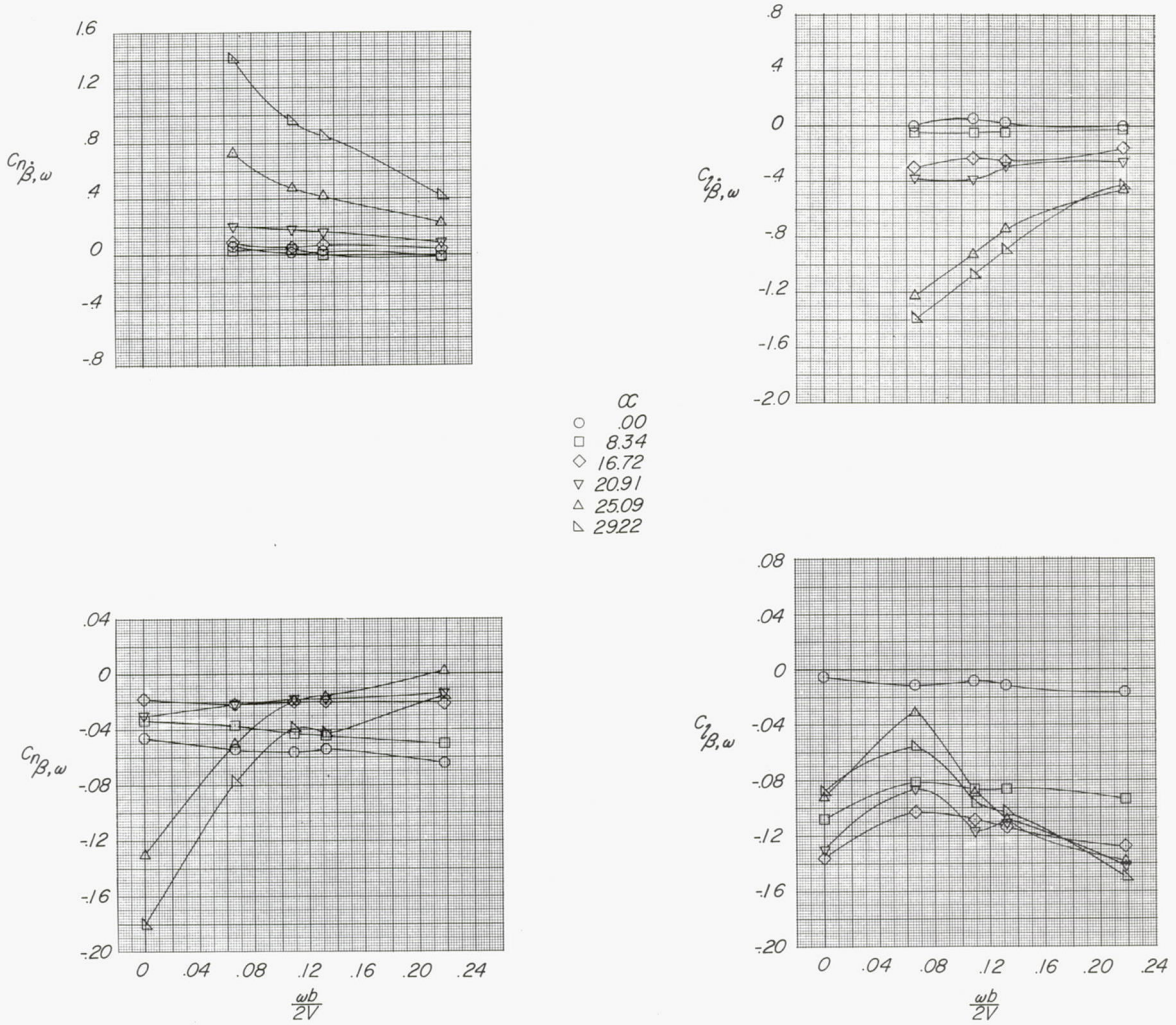

(b) Wing-fuselage configuration.

Figure 10.- Continued.

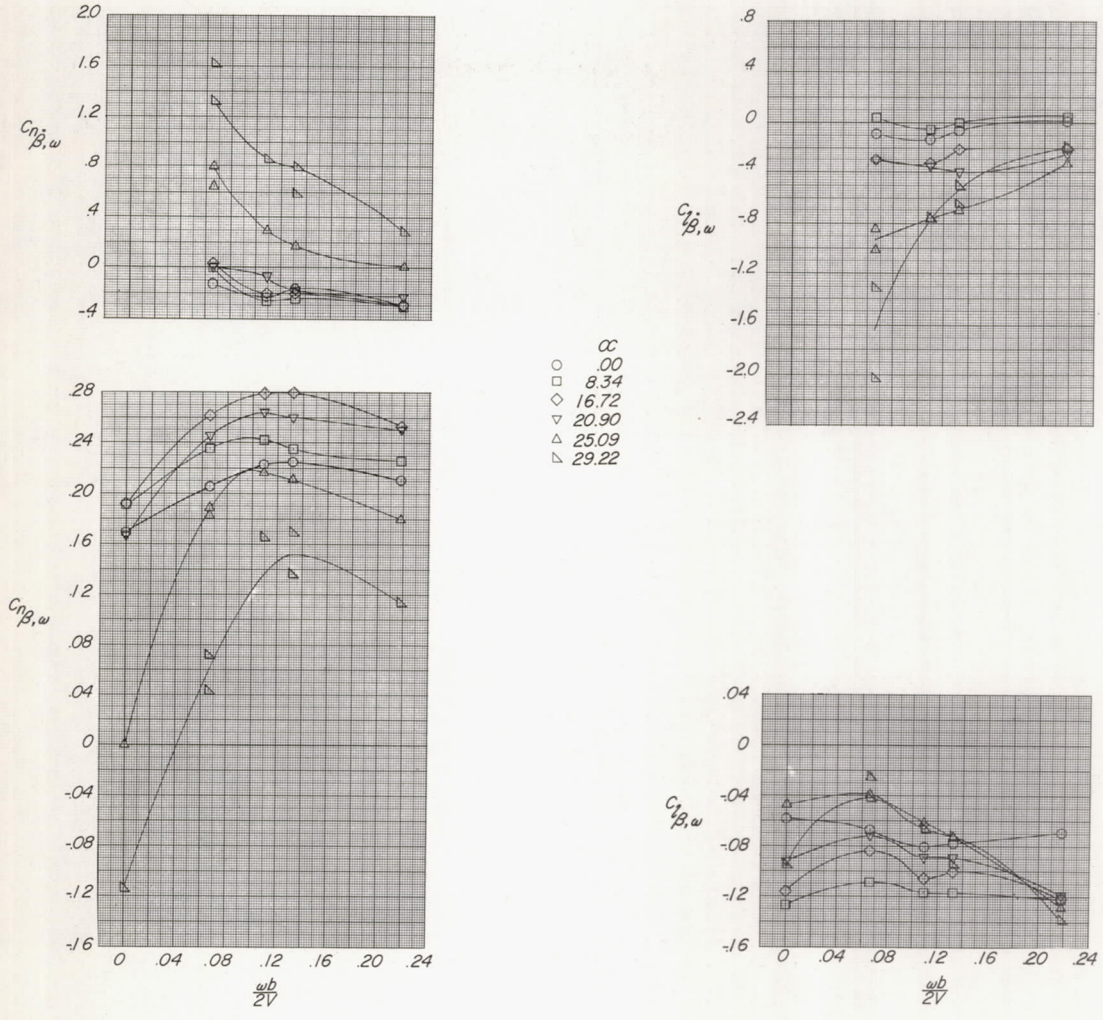

(c) Wing-fuselage-tail configuration.

Figure 10.- Concluded.

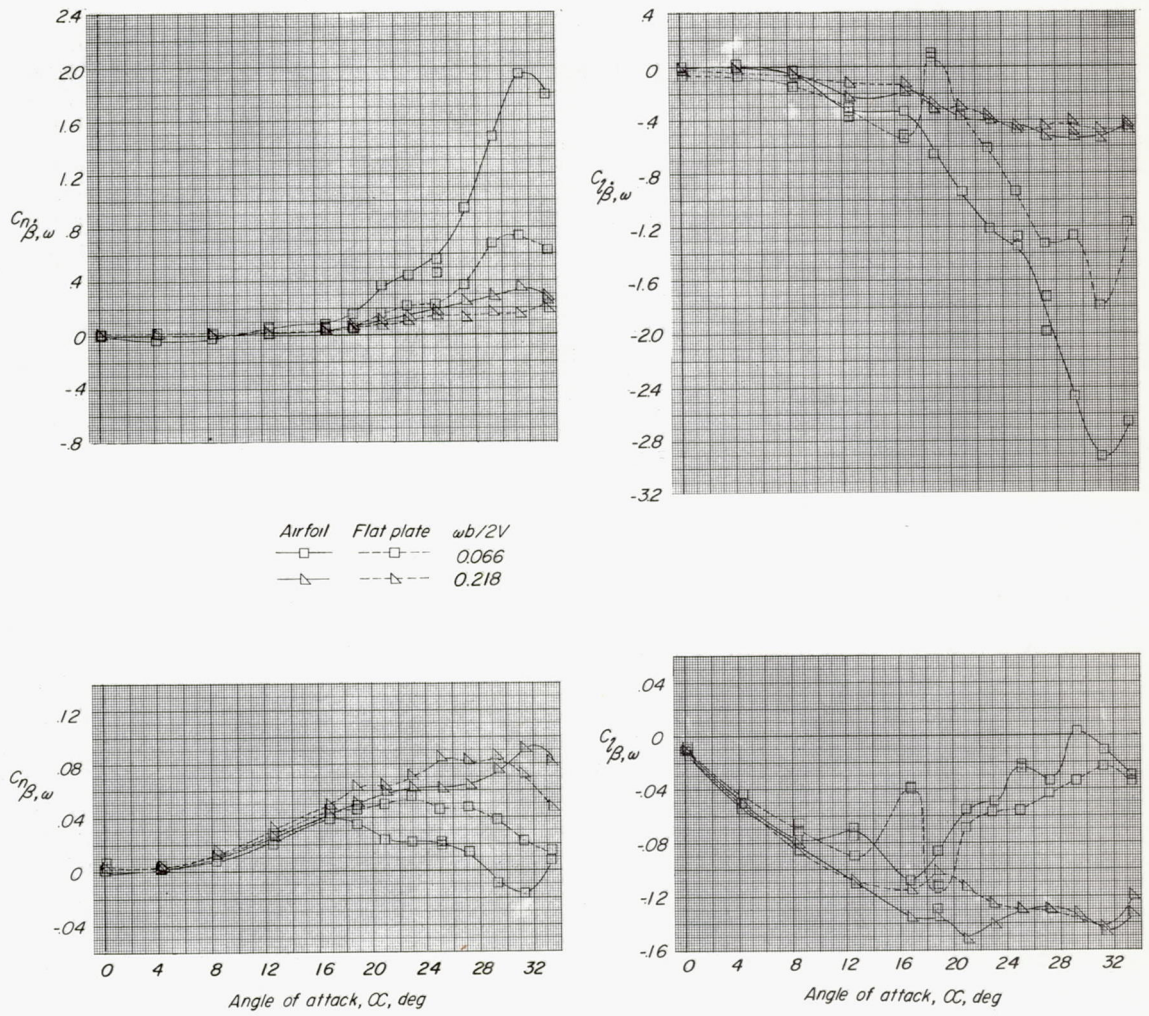

Figure 11.- Oscillation-in-sideslip stability derivatives plotted against angle of attack for the wing with a sharp leading edge (NACA 65A003 airfoil) and for the wing with a round leading edge (the flat-plate sections) for two frequencies.

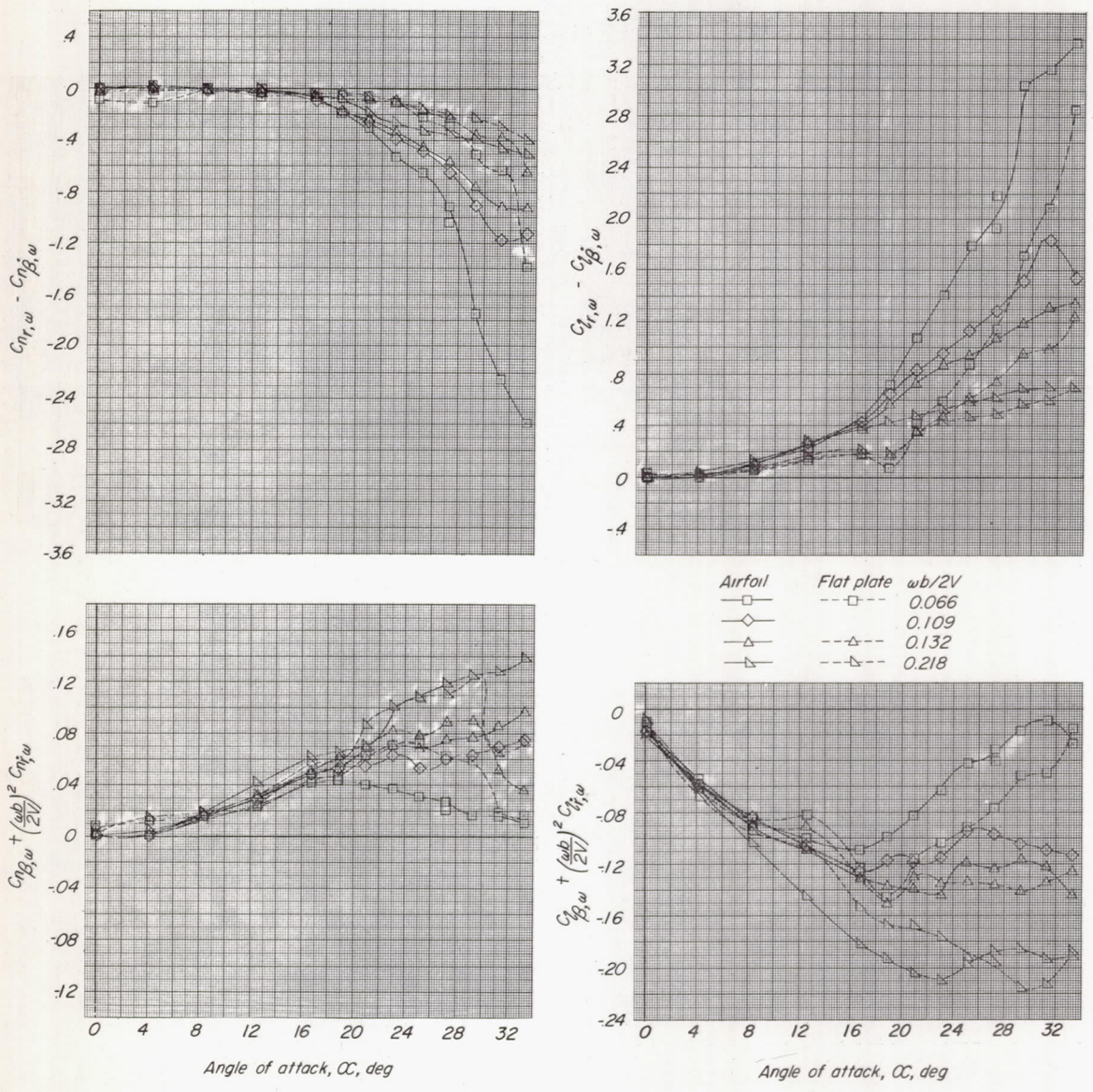

Figure 12.- Oscillation-in-yaw stability derivatives plotted against angle of attack for the wing with a sharp leading edge (NACA 65A003 airfoil) and for the wing with a round leading edge (the flat-plate sections) for various frequencies.

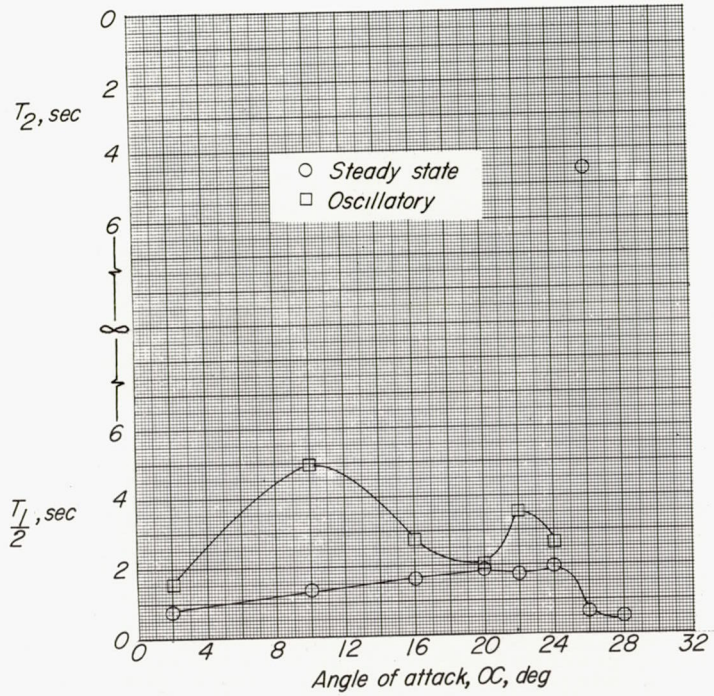

(a) Time to damp to one-half amplitude.

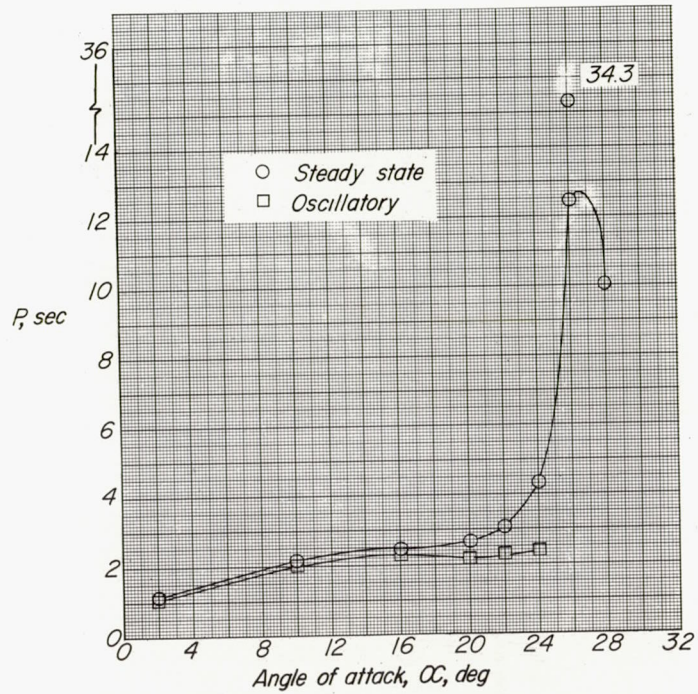

(b) Period of the oscillation.

Figure 13.- Period and time to damp to one-half amplitude of the oscillatory modes for an altitude of 0 feet.

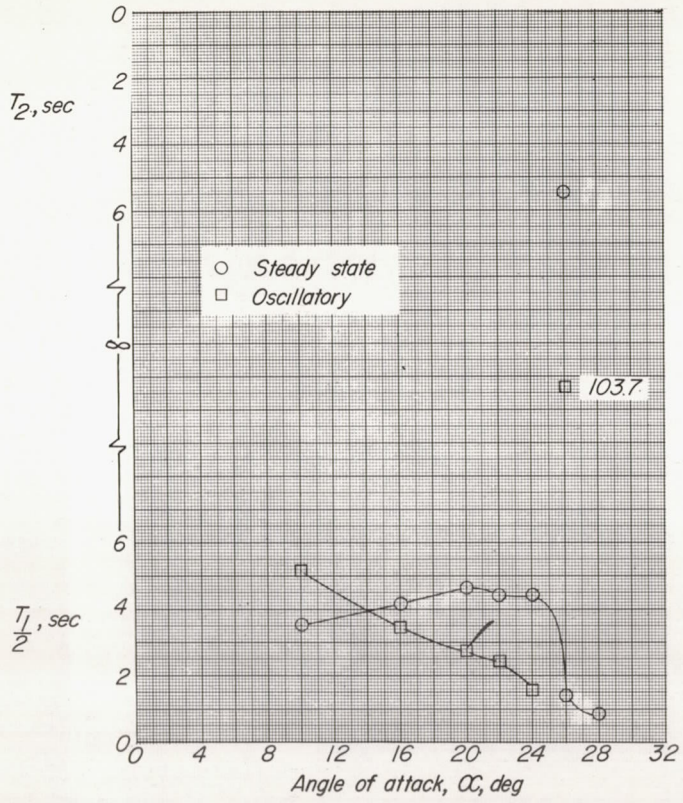

(a) Time to damp to one-half amplitude.

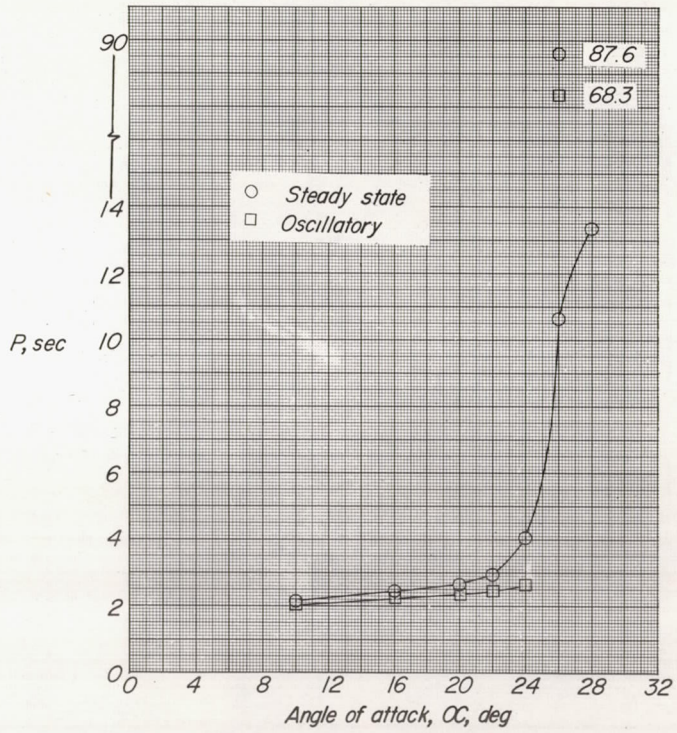

(b) Period of the oscillation.

Figure 14.- Period and time to damp to one-half amplitude of the oscillatory modes for an altitude of 50,000 feet.

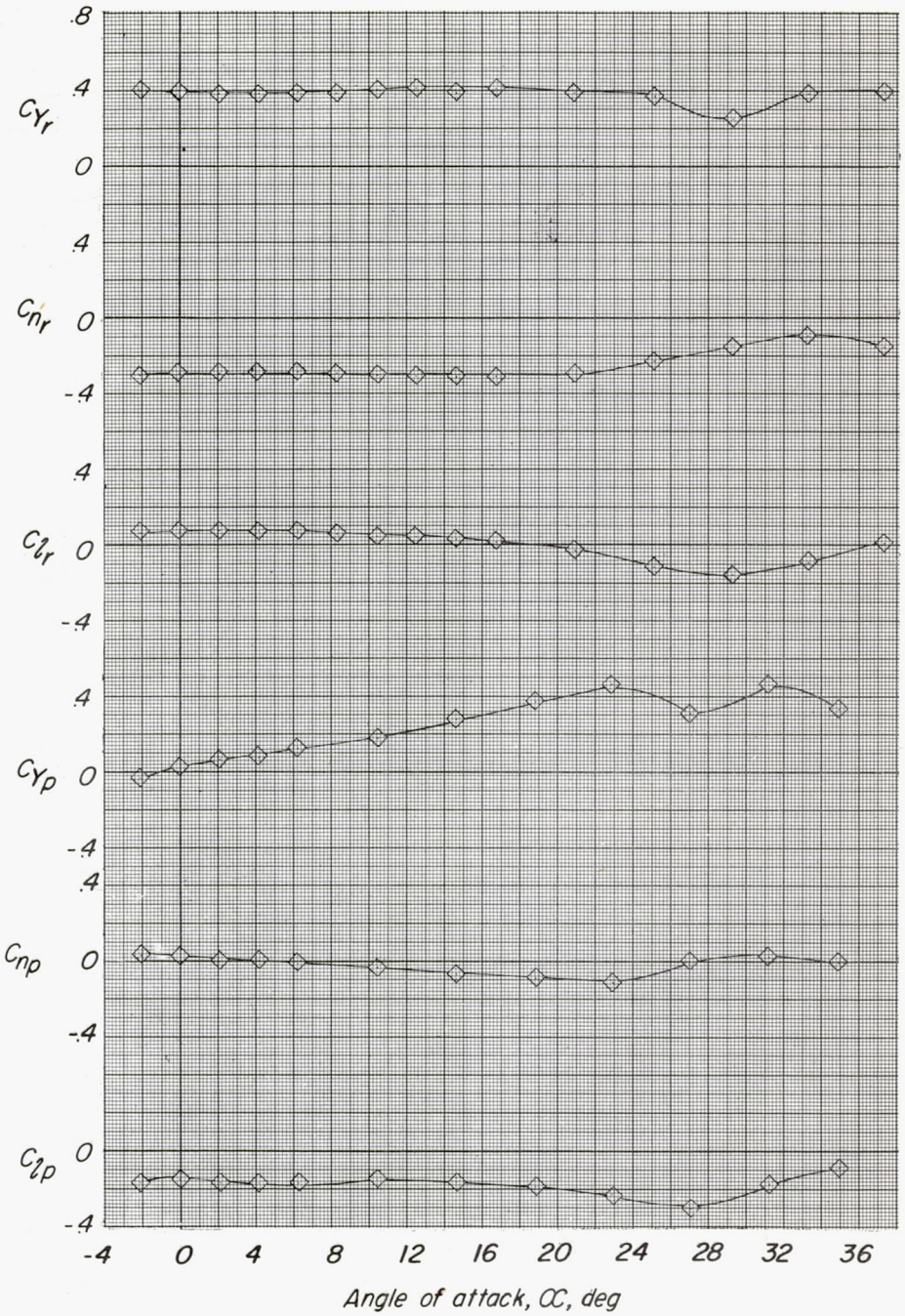

Figure 15.- Variation with angle of attack of the steady-state rolling and yawing derivatives for the wing-fuselage-tail configuration used in computations. Rolling data from reference 12 and yawing data from reference 13.